

# SYNTHESIS, CHARACTERISATION AND SOLID STATE NMR STUDIES OF 2-D AND 3-D LITHIUM- LANTHANUM / CALCIUM - TITANATES

## A DISSERTATION

*Submitted in partial fulfillment of the  
requirements for the award of the degree*

*of*

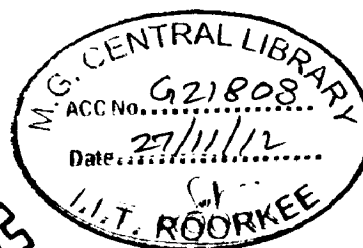
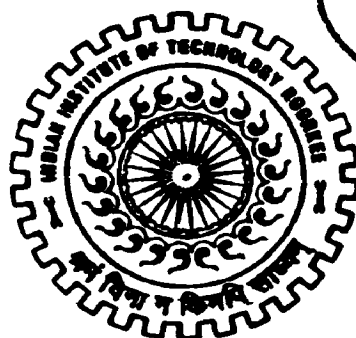
MASTER OF TECHNOLOGY

*in*

ADVANCED CHEMICAL ANALYSIS

*By*

**NISHANT GAUTAM**



DEPARTMENT OF CHEMISTRY  
INDIAN INSTITUTE OF TECHNOLOGY ROORKEE  
ROORKEE - 247 667 (INDIA)

JUNE, 2012

DEDICATED  
TO  
MY MOTHER, FATHER  
&  
GUIDE

## **CANDIDATE DECLARATION**

I, hereby, certify that the work presented in report entitled, “**SYNTHESIS, CHARACTERISATION AND SOLID STATE NMR STUDIES OF 2-D AND 3-D LITHIUM-LANTHANUM/CALCIUM-TITANATES**” has been carried out by me during the period from 1<sup>th</sup> August, 2011 to 15<sup>th</sup> June, 2012 under the supervision of Dr. Tapas Kumar Mandal, Assistant Professor of Indian Institute of Technology Roorkee.

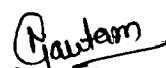


*(Dr. Tapas Kumar Mandal)*

*Assistant professor*

*Indian Institute of Technology Roorkee*

*Date 15<sup>th</sup> June*



*Nishant Gautam*

*Date: 15<sup>th</sup> June*

## ACKNOWLEDGMENT

First and foremost I want to thank my supervisor Dr. Tapas Kumar Mandal, Assistant Professor, Department of Chemistry, Indian Institute of Technology Roorkee. It has been an honour for me to be his first project fellow. He has taught me, both consciously and un-consciously, how good experimental thing is done in solid state chemistry. I heartily thank for all his contributions of time, ideas to make my dissertation work more productive and stimulating. The joy and enthusiasm he has for his research was contagious and motivational for me, even during the busy times in teaching he spend sufficient time with me for guiding me during my research work.

I would like to gratefully acknowledge the supervision and sincere support of Dr. S. Ganapathy, Emeritus Scientist, National Chemical Laboratory, Pune, in the NMR part of my dissertation work. He has spent a lot of time with us during his busy schedule. The discussions we had with him were invaluable. I specially thank him for all his support and encouragement.

It is an honour on my part to acknowledge deep gratitude to Prof. V. K. Gupta Professor and Head, Department of Chemistry, Indian Institute of Technology Roorkee, for his sustained interest and for the facilities provided in due course.

It is a great pleasure to express my sincere thanks Dr. R. K. Dutta, Assistant Professor, Department of chemistry, Indian Institute of Technology Roorkee, for his cooperation.

I would like to thank Dr. E. Viswanathan, senior research fellow, University of Madras, for his support and sharing his knowledge in Solid State NMR field.

It is a great pleasure to express my sincere thanks Dr. Manoj Kumar, Assistant Professor, Department of Metallurgy, Indian Institute of Technology Roorkee, for his cooperation.

I am also very much thankful to my lab colleague Mr. G. Naresh and Mr. Anupam Biswas for their immense cooperation and encouragement during the entire project.

My special thanks to Mr. Abdul Haq, Mr. Shiv Kumar saini, Mr. R. D. Sharma, Mr. Ravish Kumar, Mr. Madan Pal for their cooperation in the analysis of the samples.

I would like to thank Mr. Abhishek Behti, Mr. Amarkant Sharma, Mr. Amit Sharma, Mr. Ankur Sharma, Mr. Manoj Kumar, Mr. Mukesh Kumar, for their moral support.

My time at Indian Institute of Technology Roorkee, was made enjoyable in large part due to the many friends and groups that became a part of my life. I also want to thank my classmates Mr. K. P. Naidu, Mr. Ashutosh Shukla, Mr. Umesh Kumar, Mr. Bhanu Pratap Singh, Mr. Subodh Kumar, Mr. Ravikant Sharma, for spending a good time with me.

Lastly, I would like to thank my family for all their love and encouragement, For my parents who raised me with a love of science and supported me in all my pursuits.

*Date: 15<sup>th</sup> June*

*(Nishant Gautam)*

*Place: Roorkee*

## CONTENTS

	Page No.
CANDIDATE'S DECLARATION.....	i
ACKNOWLEDGEMENT.....	iii
CONTENTS.....	iv
ABSTRACT.....	v
CHAPTER 1: INTRODUCTION.....	1-15
CHAPTER 2: Synthesis and XRD characterization of Li-containing oxides with perovskite & derived structures.....	16-24
2.1 Synthesis and Characterization of $\text{Li}_{0.16}\text{La}_{0.62}\text{TiO}_3$ .....	15-16
2.2 Synthesis and Characterization of $\text{Ca}_{0.35}\text{Li}_{0.10}\text{La}_{0.40}\text{TiO}_3$ .....	17-18
2.3 Synthesis and Characterization of $\text{LiLaTiO}_4$ .....	18-19
2.4 Solid state synthesis and characterization of $\text{Li}_2\text{La}_2\text{Ti}_3\text{O}_{10}$ .....	20
2.5 X-Ray diffraction simulation and lattice parameter refinement of $(\text{Li}_{0.10}\text{Ca}_{0.35}\text{La}_{0.40})\text{TiO}_3$ .....	21-23
CHAPTER 3: Compositional Characterization/Analysis by FE-SEM	24-30
CHAPTER 4: $^6\text{Li}$ , $^7\text{Li}$ and MAS-NMR investigation of 2D and 3D Oxide	31-40
4.1 Experimental.....	32
4.2 $^6\text{Li}$ , $^7\text{Li}$ and MAS-NMR studies of $\text{Li}_{0.10}\text{Ca}_{0.35}\text{La}_{0.40}\text{TiO}_3$ .....	32-36
4.2 $^6\text{Li}$ , $^7\text{Li}$ and MAS-NMR studies of $\text{Li}_{0.16}\text{La}_{0.62}\text{TiO}_3$ .....	36-40
CONCLUSION.....	41
REFERENCES.....	42-46

## Abstract

Two- and three-dimensional (2D & 3D) perovskite based oxides containing lithium, calcium, lanthanum and titanium of known ( $\text{Li}_{0.16}\text{La}_{0.62}\text{TiO}_3$ ,  $\text{LiLaTiO}_4$  &  $\text{Li}_2\text{La}_2\text{Ti}_3\text{O}_{10}$ ) and new ( $\text{Li}_{0.10}\text{Ca}_{0.35}\text{La}_{0.40}\text{TiO}_3$ ) compositions have been synthesized. The compounds are characterized by Powder X-ray Diffraction (PXRD), Field Emission Scanning Electron Microscopy (FE-SEM) and Energy Dispersive X-ray (EDX) analysis. In  $\text{Li}_{0.10}\text{Ca}_{0.35}\text{La}_{0.40}\text{TiO}_3$  and  $\text{Li}_{0.16}\text{La}_{0.62}\text{TiO}_3$ , the Li ions are probed by static and dynamic  $^6\text{Li}$ , and  $^7\text{Li}$  NMR experiments. The results of these investigations are presented in the dissertation.

# Chapter-1

## Introduction

It is now universally recognized that gaseous emissions from the burning of fossil fuels and biomass are not only polluting the air at large, but are also creating global warming with alarming consequences (1). Moreover, a dependence on foreign oil and gas creates national vulnerabilities destroying the social stability. Therefore it is important to focus that one should concentrate more on the utilization of alternative energy sources and replacement of conventional fuel with renewable sources of energy. Solar radiation, wind, and waves represent energy sources that are variable in time and diffuse in space. These sources require energy storage. Although nuclear reactors provide a constant energy source but are associated with problems of radioactive waste disposal and other associated radiation hazards. Geothermal energy is restricted in location. However, these energy sources also benefit from electrical energy storage. The energy carriers are the electricity grid, electromagnetic waves, and chemical energy. One of the most convenient ways of energy storage is in the form of portable chemical energy.

The battery provides the portability and mobility of stored energy with an ability to deliver its chemical energy as electrical energy with high conversion efficiency and no gaseous exhaust. Moreover, among many other alternate energy sources batteries are more sought after for applications in electric vehicles. Therefore, of particular interest is a low-cost, safe, rechargeable (secondary) battery of high voltage, capacity, and rate capability.

The Li-ion batteries with high gravimetric energy density have enabled realization of the cellular telephone and lap-top computers and have transformed portable electronic devices (2). However, cost, safety, stored energy density, charge/discharge rates, and service life are issues

that continue to attract research attention (3-7). Also, there is a need for the development of the Li-battery for the potential mass market of electric vehicles to reduce CO<sub>2</sub> emission. Thus, there is enormous interest in lithium ion batteries that are safe, inexpensive, long lasting and light-weight offering high energy density. The lithium-ion battery is one of the most appealing technologies to satisfy this need.

Much attention has been paid recently to lithium ion conducting perovskites (general formula: ABO<sub>3</sub>), first reported by Latie *et al.* (8) and Belous *et al.* (9), due to their high ionic conductivity. Lanthnum-lithium-titanate (LLT) has been found to show high lithium ion conductivity, as high as 10<sup>-3</sup> S cm<sup>-1</sup> at room temperature (10). Subsequently, a lot of work has been carried out with different Li to La ratio/compostipons to investigate the crystal structure and their ionic conductivities (11). The proposed atomic models of lithium lanthanum titanate involve the ordered distribution of La ion on the perovskite A-site along the *c*-axis. The structure of these compounds differ with Li content, for higher Li content (0.06 < x < 0.14) the compound adopt tetragonal structure and for lower Li content (x < 0.06) the compound is formed in an orthorhombic structure (11, 12). Moreover for a particular compotion, the structure adopted is also a function of synthesis conditions (11).

It is found that the degree of ordered distribution of La ions is influenced by the Li content (13). This means if the Li content is high the distribution of La ions become less ordered. The distribution of La ions strongly influences the ionic conductivity because conduction of the Li ions occurs via vacancies and is percolation-controlled as La ions obstacle in the A-site sub-cell (14). In this system, La, Li and vacancies reside in the perovskite A-site, while Ti is located at the octahedral B site, and Li ions migrate between two A-sites through the vacancy. More precisely, in Li<sub>0.16</sub>La<sub>0.62</sub>TiO<sub>3</sub>, La ions and vacancies at the perovskite A-site are ordered within alternate (001) planes. The ordered arrangement of A-site cation along the *c*-axis disappears by increasing the Li content.



Attempts have been made to substitute  $\text{La}^{3+}$  by larger cations to expand the lattice that will ease the passage of lithium in the structure. Doping with monovalent cations, such as,  $\text{Ag}^+$ ,  $\text{Na}^+$  or  $\text{K}^+$  has diminished conductivity due to reduction in lithium content and disruption in ionic mobility through conducting channels (15, 16). The relationship between ionic conductivity and lattice parameter revealed that the activation energy for  $\text{Li}^+$  ion conduction decreases with the expansion of the lattice, and such behaviour could be explained by decreasing the repulsive interaction due to electron orbital overlapping between the oxide ions and the Li ions along the migration pathway (17).

Several perovskite compounds with lithium in the A-site showed high ionic conductivity of more than  $10^{-4} \text{ S cm}^{-1}$  at room temperature (18). It has been said that the presence of a vacancy in the A-site and availability of a large number of free equivalent Li-sites in the perovskite structure is responsible for high conductivity. Inaguma *et al.* have demonstrated an increase in bulk ionic conductivity in  $(\text{Li}_{0.5}\text{La}_{0.5})_{1-x}\text{Sr}_x\text{TiO}_3$ , where  $x = 0.05$ , as compared to  $(\text{Li}_{3x}\text{La}_{2/3-x})\text{TiO}_3$  system. This is in favour of the hypothesis that the lithium ionic conductivity increases with the increase in available free volume for  $\text{Li}^+$  in A-site (18). The evidence that the LLTO compounds having smaller  $\text{Ln}^{3+}$  showed lower lithium ionic conductivities than those of  $(\text{Li}_{1/2}\text{La}_{1/2})\text{TiO}_3$  also favour the above hypothesis. However, for higher doping levels of Sr, for example, in  $\text{La}_{0.375}\text{Li}_{0.375}\text{Sr}_{0.25}\text{TiO}_3$ , the conductivity reduces substantially, which is contradictory to the above hypothesis. Similar results are observed in the Ba-doped LLTO compounds with a rapid reduction in Li-ion conductivity. Therefore, it is likely that other secondary factors may also have an influence on the conductivity that are unknown at the present level of understanding of lithium ion conduction in LLTO and related compounds (11).

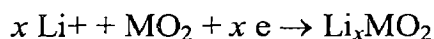
High lithium ion conductivity has also been reported for other rare earth ( $\text{Ln}^{3+}$ ) substituted perovskite titanates  $\text{Li}_{0.5}\text{Ln}_{0.5}\text{TiO}_3$  ( $\text{Ln} = \text{La}, \text{Pr}, \text{Nd}, \text{Sm}$ ) (19). On substitution of  $\text{Ln}^{3+}$ , the

symmetry of the lattice changed from cubic  $\text{Li}_{0.5}\text{La}_{0.5}\text{TiO}_3$  to orthorhombic (for  $\text{Ln} = \text{Pr}, \text{Nd}, \text{Sm}$ ) with a consequent decrease in the lithium ion conductivity. This has been attributed to the decreased size of the Ln cations which reduces the size of bottleneck where the Ln ions themselves acts as spacer for lithium ion conduction (19). Inaguma *et al.* (20) have also shown that the conductivity in LLTO is strongly dependent not only on the concentration but also the arrangement of A-site ions. The dependence of activation energy for ion conduction both on the covalency of B-O bond and bottleneck size have also been pointed out. Further, there is a difference in ionic conductivity between the furnace-cooled and quenched samples; while a higher degree of order is achieved in furnace cooled samples, quenched sample showed a lower degree of order in  $\text{Li}_{3x}\text{La}_{3/2-x}\text{TiO}_3$  system (21). The conductivity at 300 K of the furnace-cooled sample is approximately three times higher than that of the quenched sample. A maximum bulk conductivity of  $1.53 \times 10^{-3} \text{ S cm}^{-1}$  at 25 °C was the best reported conductivity till then for a perovskite solid solution,  $\text{Li}_{3x}\text{La}_{3/2-x}\text{TiO}_3$ , where  $x = 0.12$  (21).

## **Basics of Lithium ion Batteries**

The reactions that occur in normal batteries are irreversible, so they could not be recharged and reused. Rechargeable lithium batteries involve a reversible insertion/extraction of lithium ions (guest species) into/from a host matrix (electrode material), called lithium insertion compound, during the discharge/charge process. The lithium insertion/extraction process occurring with a flow of ions through the electrolyte is accompanied by the reduction/oxidation reaction of the host matrix combined with a flow of electrons through the external circuit. Murphy *et al.* studied the lithium intercalated compounds based on rutile

structure way back in 1978 (22). The cathodic electrochemical reaction that occurs during lithiation can be represented as:

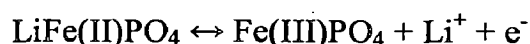


A general intercalation/de-intercalation process that forms the basis of rechargeable lithium batteries can be represented by the following reaction,



The name of the lithium-ion battery is usually determined by cathode material, for example, lithium iron phosphate ( $\text{LiFePO}_4$ ) and lithium cobalt oxide ( $\text{LiCoO}_2$ ) battery, where the cathode materials are made up of ( $\text{LiFePO}_4$ ) and ( $\text{LiCoO}_2$ ), respectively.

In the case of lithium iron phosphate batteries ( $\text{LiFePO}_4$ ), lithium iron phosphate ( $\text{LiFePO}_4$ ) is the cathode,  $\text{Li}_x\text{C}_6$  is the anode, and the electrolyte is a non-aqueous solution. The  $\text{LiFePO}_4$  has an olivine structure. During discharge, the lithium ions are inserted into the van der Waals gap between the olivine structure and the charge balance is maintained by a reduction of the  $\text{Fe}^{3+}$  ions to  $\text{Fe}^{2+}$ . The insertion/extraction reaction of the lithium ions is represented as



During charging, exactly the reverse process involving the extraction of lithium from the van der Waals gap and oxidation of  $\text{Fe}^{2+}$  to  $\text{Fe}^{3+}$  occurs. Figure 1 shows the illustration of the charge / discharge process in a lithium-ion cell (23).

## Battery Components

There are three important components of a battery namely cathode, anode and electrolyte. The materials used for cathode, anode and electrolyte are lithium metal oxide powder, graphite powder and lithium salt-organic solvents, respectively. Each of the battery components has their own function. Cathode emits Li-ion to the anode during charging and receives the Li-ion during discharging. The reverse phenomenon takes place at the anode

during the charge-discharge process of a battery. Electrolyte helps to transport the Li-ions from cathode to anode and vice-versa.

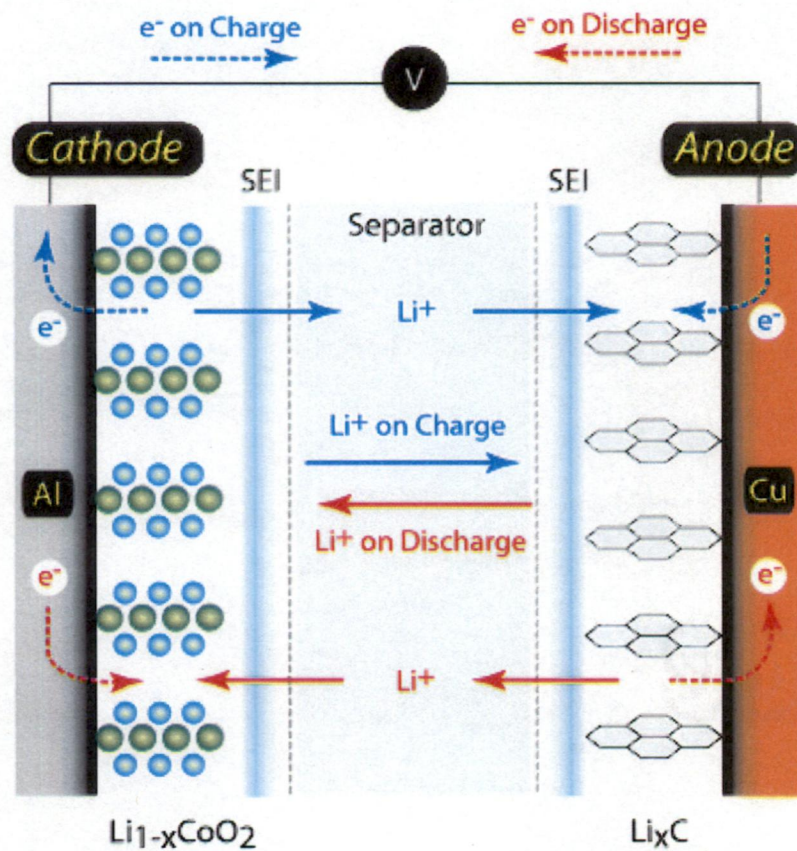


**Figure 1.1** Charge/discharge process in a lithium ion cell (23).

## Cathode

The cathode is one of the key components in the battery pack. The cathode consists of current collector made up of 20 $\mu\text{m}$  thick Aluminium foil (23). In lithium ion battery, the state-of-the-art cathode materials comprise of lithium cobalt oxide ( $\text{LiCoO}_2$ ), lithium manganese oxide ( $\text{LiMn}_2\text{O}_4$ ), lithium nickel-cobalt-manganese oxide [ $\text{Li}(\text{Ni}_x\text{Co}_y\text{Mn}_z)\text{O}_2$ ], vanadium oxides, olivines (e. g.,  $\text{LiFePO}_4$ ) and rechargeable lithium oxides (24, 25). The lithium cobalt and

lithium nickel oxide systems with a layered structure are the most widely investigated cathode materials for lithium batteries. The lithium cobalt oxide battery released by Sony in 1990 is the most common commercially used battery in electronic devices due to its high energy density. But, the development of alternate cathode materials is necessary due to the high raw materials cost, instability and toxic features of the lithium cobalt oxide. In 1996, Prof. John B. Goodenough and co-workers at the University of Texas at Austin identified lithium iron phosphate ( $\text{LiFePO}_4$ ) and related materials with olivine structure as cathode materials (26). This discovery is recognised as a breakthrough technology in the field of rechargeable battery because the stable olivine crystal structure could not only provide longer cycle life but satisfy higher safety standards. Moreover, the materials cost was much lower due to the cheaper iron component instead of expensive cobalt, nickel and manganese.

## **Anode**

The anode is usually made of graphite with a thin coating of copper foil. In case of graphite anode, a single lithium ion can be inserted per each hexagon in the graphitic molecular structure. The theoretical capacity of graphite is 372 mAh/g. However, this is considered to be poor as compared to the charging density of lithium (3862 mAh/g). Due to this, a considerable amount of research effort have been devoted to increase the capacity by using novel carbon, metal alloys, and other intermetallic compounds. The best carbons in current literature can intercalate 2.5 Li ions and achieve capacities as high as 750 mAh/g. Several works have been carried out on alloys and carbon-coated alloy systems (27-30). Liu *et al.* (30) have demonstrated that copper-tin alloys could provide a capacity of 460 mAh/g even up to 40 cycles. Although, the alloy and intermetallic systems show high capacity, but have poor cycleability due to dramatic volume changes. A very high capacity of 4199 mAh/g is shown by silicon with a composition of  $\text{Si}_5\text{Li}_{22}$  (31). It is interesting to note that the average voltage

of silicon (0.5 ~ 1V) is higher than that of graphite. However, in silicon the capacity loss leads to poor cycling behaviour.

## **Electrolyte**

The main task of the electrolyte in lithium ion battery is to continuously transport lithium across anode and cathode during charge/discharge. The basic requirements of a suitable electrolyte are high Li-ion conductivity, low melting and high boiling points, chemical and electrochemical stability and safety. The two main type of electrolyte are: (1) Liquid electrolyte; (2) Solid electrolyte.

### *(1) Liquid electrolytes:*

Liquid electrolyte consists of lithium salts, such as  $\text{LiPF}_6$ ,  $\text{Li}[\text{PF}_3(\text{C}_2\text{F}_5)_3]$ , or  $\text{LiBC}_4\text{O}_8$  in organic solvents, such as ethylene carbonate (EC), dimethyl carbonate (DMC), and diethyl carbonate (DEC) (32). The general liquid electrolyte is a 1 molar solution of a lithium salt in an organic solvent. Above the 1 molar concentration of liquid electrolyte, there is significant salt precipitation at low temperatures. Due to the safety concerns organic solvents, which would decompose under high voltage operation, are not suitable for wide applications.

### *(2) Solid electrolytes:*

Solid electrolyte offers several advantages, including enhanced safety (no liquid to spill), lighter weight, and design flexibility but their higher internal resistance limit their performance and lifetime. Additionally, they show very poor low temperature performance because the lithium mobility in the solid is greatly reduced at low temperatures.

A wide variety of metal oxides are known to exhibit high bulk lithium ion conductivity. Considering their ionic conductivities as a function of temperature, they can be divided mainly into two groups: (i) high-temperature ionic conductors, for example,  $\text{Li}_2\text{SO}_4$ - $\text{Li}_4\text{SiO}_4$  system (33), and  $\text{Li}_{14}\text{ZnGe}_4\text{O}_{16}$  (Lithium Super Ionic Conductor, LISICON) (34); and (ii) low-temperature ionic conductors, for example,  $\text{Li}_{3.6}\text{Ge}_{0.6}\text{V}_{0.4}\text{O}_4$  (35),  $\text{Li}_{1.3}\text{Al}_{0.3}\text{Ti}_{1.7}(\text{PO}_4)_3$  (36), and A-site deficient perovskite solid solution,  $\text{Li}_{0.35}\text{La}_{0.55}\text{TiO}_3$  (10).

According to the type of compounds, these electrolytes can also be categorized into four groups. These are

- (i) Lithium oxy-acid salts, for example,  $\text{Li}_2\text{SO}_4$  -  $\text{Li}_4\text{SiO}_4$  system.
- (ii)  $\gamma$ - $\text{Li}_3\text{PO}_4$  solid solutions, for example, LISICON and  $\gamma$ - $\text{Li}_{3.6}\text{Ge}_{0.6}\text{V}_{0.4}\text{O}_4$ .
- (iii) NASICON-structured  $\text{Li}_{1.3}\text{Al}_{0.3}\text{Ti}_{1.7}(\text{PO}_4)_3$ .
- (iv) Li-ion conducting A-site deficient perovskite solid solution (Li-ADPESS).

There are several other systems that have recently been investigated as solid electrolytes are thio-LISICONs ( $\text{Li}_{3.25}\text{Ge}_{0.25}\text{P}_{0.75}\text{S}_4$ ) (37), glass ceramics (38, 39) ( $\text{Li}_7\text{P}_3\text{S}_{11}$ ) and glassy materials ( $\text{Li}_2\text{S}$ - $\text{SiS}_2$ - $\text{Li}_3\text{PO}_4$ ) (40, 41). All the above materials show ionic conductivities of the order of  $10^{-3}$  S  $\text{cm}^{-1}$ . Recently, a lithium superionic conductor,  $\text{Li}_{10}\text{GeP}_2\text{S}_{12}$ , with a three dimensional framework structure and an extremely high lithium ion conductivity of  $12 \times 10^{-3}$  S  $\text{cm}^{-1}$  at room temperature, have been reported (42). To date, the known fastest lithium ion-conducting solid oxide electrolytes are the perovskite-type ( $\text{ABO}_3$ ) oxides, such as, lithium lanthanum titanates (LLTO)  $\text{Li}_{3x}\text{La}_{(2/3)-x}\text{TiO}_3$ , and structurally related materials, with A = Li, La and B = Ti.

## LLTO Solid Electrolytes

Solid-state  $\text{Li}^+$ -ion conductors are extensively studied because of their applications in high-energy density lithium-ion batteries and other electrochemical devices. Up to now, one of the most performing Li-ion conductors is a lithium-lanthanum titanate perovskite,  $\text{Li}_{3x}\text{La}_{3/2-x}\text{TiO}_3$  for  $x = 0.12$ , (21) as mentioned earlier. The perovskite phase was first reported by Vallino and Mazza during a study on the ternary system  $\text{La}_2\text{O}_3\text{-Li}_2\text{O-TiO}_2$  and it was shown to have a variable compositional range,  $\text{La}_{2/3-x}\text{Li}_{3x}\text{TiO}_3$  for  $0.04 < x < 0.14$  even at that time (43). Later on, the ionic conductivity and structural analysis of this lithium ionic conductor was reported by Kawai *et al.* (44) and Robertson *et al.* (45), respectively, and more recently by Fourquet *et al.* (13). A structural model based on  $P4/mmm$  space group has been proposed. According to this model,  $\text{La}^{3+}$  and vacancies are situated at the centres of the 12-coordinated perovskite cage. Though the assignment of the 12-coordinated site for the location of  $\text{La}^{3+}$  and vacancies are accepted by all authors, but the location of the  $\text{Li}^+$  ions in this structure is still controversial. Moreover, local ordering inside this crystalline structure can arise by the non-uniform distribution of  $\text{La}^{3+}$ ,  $\text{Li}^+$  and vacancies among the A sites of the perovskite lattice. Figure 1.2 shows the lithium-lanthanum titanate perovskite structures with ordered and disordered arrangement of  $\text{Li}^+$  and  $\text{La}^{3+}$  cations in  $\text{Li}_{0.16}\text{La}_{0.62}\text{TiO}_3$  and  $\text{Li}_{0.5}\text{La}_{0.5}\text{TiO}_3$ , respectively (11).

The Li-ion motion in the perovskite oxides,  $\text{Li}_{3x}\text{La}_{3/2-x}\text{TiO}_3$ , is strongly affected by the oxygen environment and the distribution of lanthanum and vacancies. The Li-ion motion in this relatively simple structure occurs *via* different pathways and accordingly a distribution of activation energies exist. However, it is well known that the dc-bulk conductivity is only due to the passage of Li ion from one A-site to a neighbouring vacant site. The bulk and grain-boundary ionic conductivities of the perovskite LLTO are in the range  $10^{-3} \text{ S cm}^{-1}$  and  $10^{-4} - 10^{-5} \text{ S cm}^{-1}$ , respectively, at room temperature. These values are comparable with those of



the commonly used liquid electrolytes. However, the electronic conduction which arises due to the reduction of  $\text{Ti}^{4+}$  to  $\text{Ti}^{3+}$  in these bulk conductors with the intercalation of lithium precludes the use of this oxide as solid electrolyte.

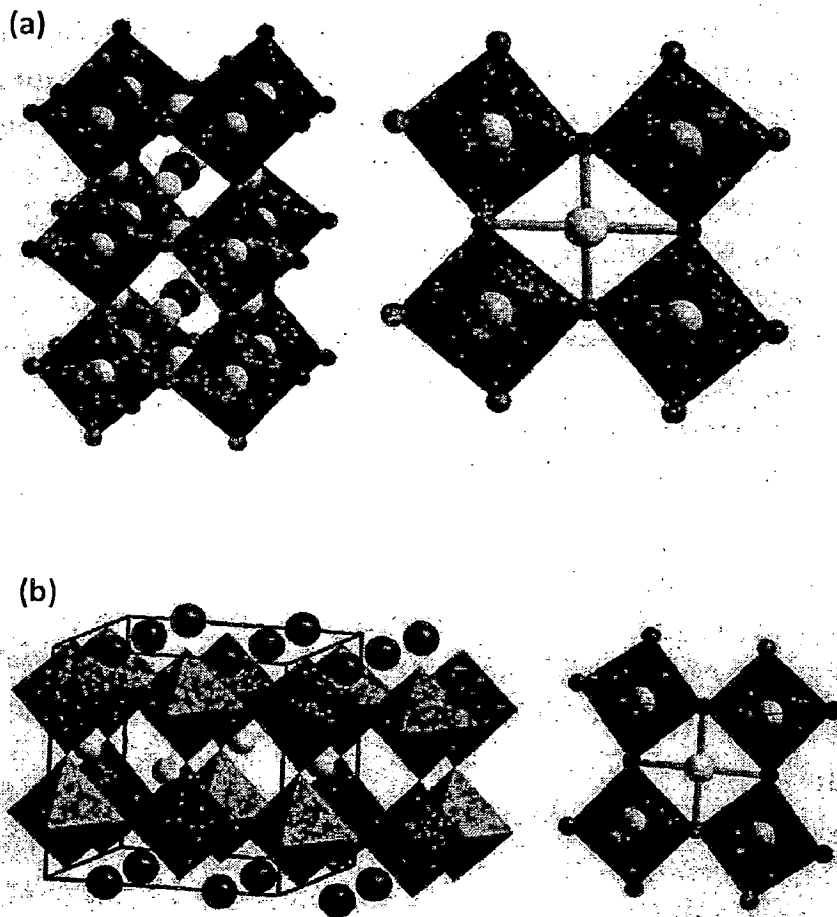


Figure 1.2 shows the lithium-lanthanum titanate perovskite structures with disordered and ordered arrangement of  $\text{Li}^+$  and  $\text{La}^{3+}$  cations in (a)  $\text{Li}_{0.5}\text{La}_{0.5}\text{TiO}_3$  and (b)  $\text{Li}_{0.16}\text{La}_{0.62}\text{TiO}_3$  (11).

## Li-NMR

Li NMR has played an important role in the study of cathode materials used in rechargeable lithium-ion batteries (46, 47). This is due to the fact that in solid state NMR of Li-ions the local environment of Li that are directly involved in the conduction and thus in electrochemical processes can be probed. Due to the very narrow chemical shift range of Li-NMR it is often impossible to distinguish resonances corresponding to different local chemical environments in diamagnetic materials. However, at higher field strengths, it may occasionally be possible to resolve the spectra (48, 49). Moreover, often the Li-NMR spectra are strongly influenced by larger interactions. For example, quadrupolar coupling (for  ${}^6\text{Li}$ ,  $I = 1$ ;  ${}^7\text{Li}$ ,  $I = 3/2$ ) dominate in diamagnetic samples while the hyperfine interaction with unpaired electrons take over in paramagnetic samples (47). Among the two Li nuclei,  ${}^7\text{Li}$  has higher natural abundance and a larger quadrupolar moment while  ${}^6\text{Li}$  is less abundant and a smaller quadrupolar moment. Due to smaller interaction of the quadrupolar nucleus with the electric field gradient (EFG) at the nucleus,  ${}^6\text{Li}$  results in high resolution spectra and characteristic broadening in the static NMR. But, in case of  ${}^7\text{Li}$  a series of spinning side bands are observed due to satellite transitions in the magic angle spinning (MAS) NMR experiments. This anisotropic interaction is very informative in terms of distinguishing between ions in symmetric and more distorted environments (47).

The motional narrowing of the NMR line shape as a function of temperature can shed light on nuclei at different spin environments as well as the mobility of the lithium ions in the structure (50). Spin-lattice relaxation rate measurements as a function of temperature can also help to understand the relaxation mechanisms and diffusion of atoms / ions in solids (51, 52). The NMR line shape is additionally influenced by the quadrupolar interaction in case of  ${}^7\text{Li}$ , especially when the nucleus is in a low crystal symmetry site (50).

The knowledge about reliable diffusion parameters of  $\text{Li}^+$  ions in solid electrolytes plays an important role not only in the field of battery development, but the diffusion phenomenon itself, which occurs everywhere in nature and of great interest in physical chemistry and materials science (53). Moreover, the study of Li self-diffusion parameters over long distances from an atomic point of view is of great interest. This can be carried out with the help of microscopic techniques (54). Also, Li self-diffusion parameters can be obtained by using  $^6,7\text{Li}$  spin alignment echo (SAE) NMR spectroscopy (55, 56). A large number of polycrystalline and glassy materials have been investigated by SAE NMR spectroscopy (55, 56). It is interesting to note that, in many cases the results are in corroboration with those obtained from macroscopic techniques, (57, 58), such as field-gradient NMR or dc-conductivity measurements. Besides, there exists only a few other macroscopic methods that are sensitive to long-range lithium transport parameters. Moreover, SAE NMR spectroscopy can be used for extremely slow diffusion processes characterized by jump rates down to a few jumps per minute (56). The SAE-NMR technique serves as an easily applicable tool to study ultra-slow Li dynamics. These measurements were usually performed at relatively low temperatures, which is very beneficial for heat-sensitive materials. The study of slow diffusion can also be achieved by the use of  $^6\text{Li}$  high-resolution magic angle spinning (MAS) 2D exchange NMR spectroscopy, which can additionally provide valuable information about site-specific jump rates (59).

Finally, the identification of new ion conductors, which is greatly driven by the demand for developing clean-energy storage systems, requires the detailed atomic scale measurement of Li-ion diffusion parameters. For example, Li transport processes play a crucial role during the charging and discharging of a lithium-ion battery. Li SAE NMR spectroscopy, which complements the large set of methods to probe lithium diffusion parameters, is expected to be

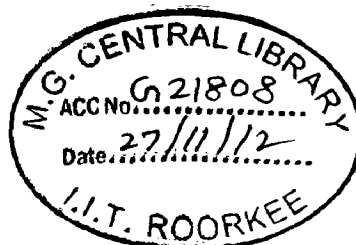
a very helpful tool to promote the target-oriented development of solid ion conductors suitable for use as electrodes or electrolytes.

Li-NMR investigations of Li-ion dynamics in the perovskite based lithium-lanthanum-titanate (LLTO) solid solution has been reported in the recent literature (60, 61). Emery *et al.* have shown that two slightly different Li environments are present in the  $\text{Li}_{3x}\text{La}_{2/3-x}\square_{1/3-2x}\text{TiO}_3$  perovskite fast ion conductors (60). The two types of lithium also differ in their motion; while one is faster with a frequency of  $\sim 100$  MHz at 350 K, the other one is slower with a frequency of  $\sim 60$  MHz at 280 K. The motions are attributed to Li-ion hopping between the cages of the A-site in the perovskite structure (60). Temperature dependent T1 & T2 relaxation time measurements in  $\text{Li}_{0.18}\text{La}_{0.61}\text{TiO}_3$  perovskite have indicated two main relaxation mechanisms (61). While one has been ascribed to localized exchanges (200 – 273 K), the other one corresponds to extended motions of Li (above 273 K). Based on their NMR and conductivity studies, the authors propose correlated ion motions in this oxide.

In this dissertation work, we have aimed at synthesizing known and new 3-D perovskite based oxides, namely, (Li, La)TiO<sub>3</sub> and (Li, Ca, La)TiO<sub>3</sub>, in addition to other known 2-D layered perovskites where the perovskite block thickness are varied from one to other. This modifies the local Li-ion environment in all the members. The compounds thus provide different Li-ion environment and can be probed by Solid State Li NMR.

Although the substitution of Sr and Ba at the (Li, La) site of the LLTO has been carried out, but the Ca analogues have not been investigated. Moreover, considering the dependence of ionic conductivity on cell volume, we thought that the substitution of Ca at the La-place will not affect the cell volume significantly while allowing us to vary the Li-ion and vacancy concentration. Our aim is to synthesize the Ca-substituted LLTO members together with some of 2D perovskites and carry out the structural and compositional characterization of all the compounds. Then all the compounds will be subjected to Li-NMR experiment, wherein

we can probe the local Li environment as well as comment on the mobility of Li-ion in the materials/structure types. This study in turn can help, in an efficient way, understand the mechanism of Li-conduction and establish structure-property correlation of novel Li-oxides for the better design of anode, cathode, and electrolyte materials based on Li (62).



## Chapter-2

### Synthesis and XRD characterization of Li-containing oxides with perovskite & derived structures

The perovskite type compounds have the composition  $ABO_3$ . This  $ABO_3$  composition can adopt a large number of structures depending on the relative size of A and B cations and chemical bonding, such as perovskite, pyrochlore and ilmenite, which are mostly based on  $BO_6$  octahedra network. Other varieties of structures, for example, layered variants of perovskites exists when  $ABO_3$  interstacks with rock salt, (AO), type compounds, forming  $A_{n+1}B_nO_{3n+1}$  a series of compounds known as Ruddlesden-Popper (RP) phases. The  $ABO_3$  composition consists of a three dimensional (3D) framework of corner sharing octahedra in which the A-cation resides on the dodecahedral sites surrounded by twelve oxide ions. In perovskite some symmetry lowering distortion occurs when the size of A and B cation are not equal. The flexibility of the perovskite towards a wide variety of substitution at both A-type and B-type cation give rise to a very large number of perovskite derived structures.

In this dissertation work we are mainly focused in the synthesis and characterization of perovskite and some layered perovskite structure.

#### 2.1 Synthesis and Characterization of $Li_{0.16}La_{0.62}TiO_3$

The  $Li_{0.16}La_{0.62}TiO_3$  was synthesized by a conventional solid-state reaction. (63) The starting materials were  $La_2O_3$  (4N),  $Li_2CO_3$  (3N), and  $TiO_2$  (3N). The raw material  $La_2O_3$  (99.99%) from CDH analytical reagent,  $Li_2CO_3$  (99.99%) Sigma Aldrich, and  $TiO_2$  (99.99%) from CDH analytical reagent were used. A mixture of the raw materials (the molar ratio of metals was La :Li : Ti-0.6 : 0.2 : 1) was first calcined at 800 °C for 4 h, 1150 °C for 28 h, and 1250

°C for 12 h in air with intermediate grindings following the procedure was reported in the literature (63). The calcined powder was pressed into pellets and sintered at 1350 °C for 6h in air and then furnace-cooled. Purity of the phases was ascertained by powder X-ray diffraction (XRD) and comparison with standard diffraction data files (JCPDS).

Powder XRD patterns were recorded using a Bruker D8 Advanced X-ray powder diffractometer using Cu K $\alpha$  radiation in the 2 $\theta$  range 5-80° at a scan speed of 4°/min. Figure 2.1 shows the XRD pattern of nominal Li<sub>0.16</sub>La<sub>0.62</sub>TiO<sub>3</sub>. Comparison of the observed XRD data with the reported database files (JCPDS) compares excellently with that of Li<sub>0.125</sub>La<sub>0.625</sub>TiO<sub>3</sub> (card no. # 47-0669) is indicating the formation of single phase compound.

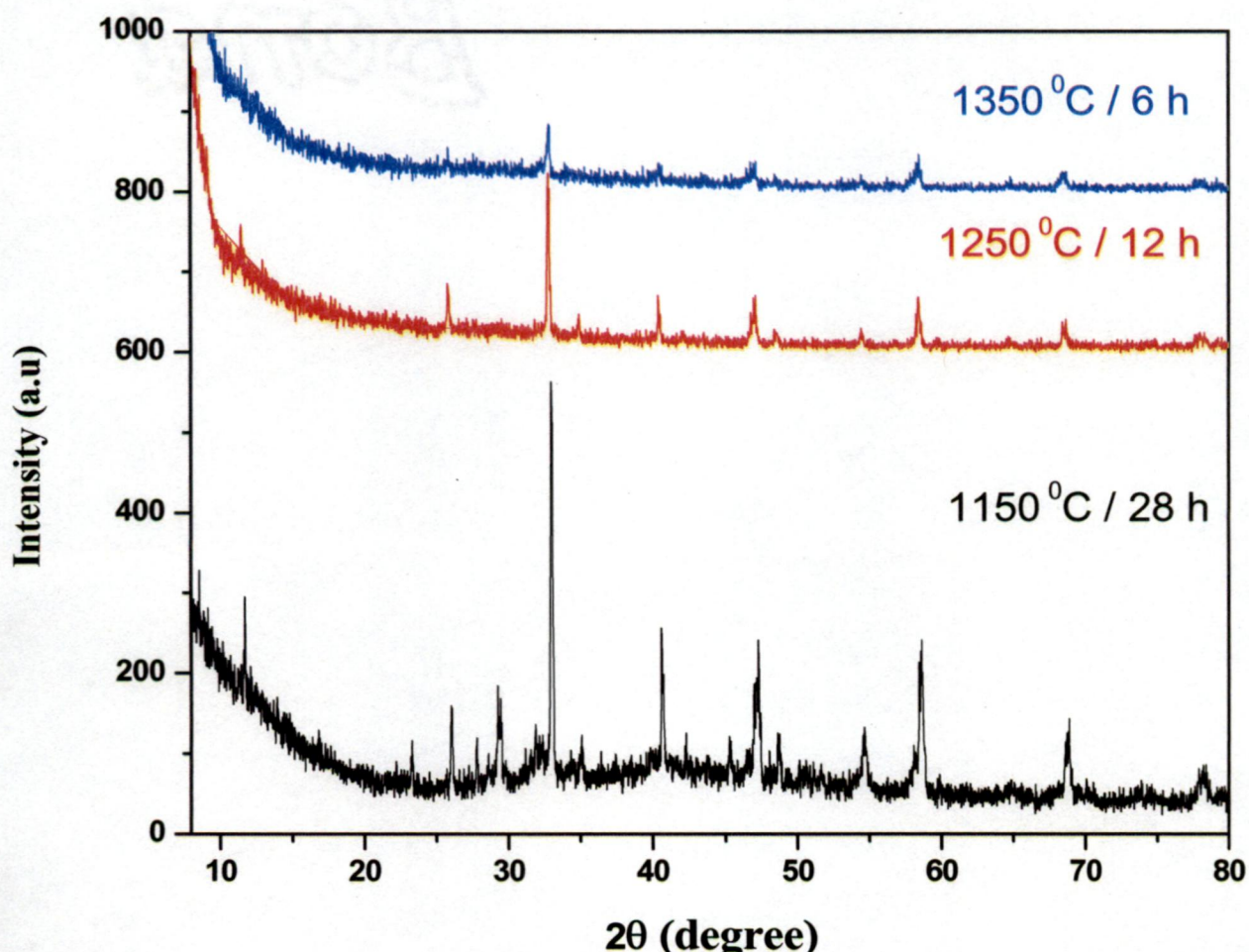


**Figure 2.1** Powder XRD patterns of nominal Li<sub>0.16</sub>La<sub>0.62</sub>TiO<sub>3</sub> at different temperatures.

## 2.2 Synthesis and Characterization of $\text{Li}_{0.10}\text{Ca}_{0.35}\text{La}_{0.40}\text{TiO}_3$

The  $\text{Li}_{0.10}\text{Ca}_{0.35}\text{La}_{0.40}\text{TiO}_3$  was synthesized by a conventional solid-state reaction. The starting materials were  $\text{La}_2\text{O}_3$ ,  $\text{Li}_2\text{CO}_3$ ,  $\text{CaCO}_3$  and  $\text{TiO}_2$ . The raw materials  $\text{La}_2\text{O}_3$  (99.99% from CDH analytical reagent),  $\text{Li}_2\text{CO}_3$  (99.99% from Sigma Aldrich), and  $\text{TiO}_2$  (99.99% from CDH analytical reagent) were used. A mixture of the raw materials (the molar ratio of metals was Ca: La :Li : Ti-0.4 : 0.35 : 0.15: 1) was first calcined at 800 °C for 4 h, 1150 °C for 28 h, and 1250 °C for 12 h in air with intermediate grindings. The calcined powder was pressed into pellets and sintered at 1350 °C for 6h in air and then furnace-cooled. Purity of the phases was ascertained by XRD and comparison with standard diffraction data files (JCPDS). Figure 2.2 shows the XRD pattern of nominal  $\text{Li}_{0.10}\text{Ca}_{0.35}\text{La}_{0.40}\text{TiO}_3$  after heating at 1150 °C and 1250 °C.

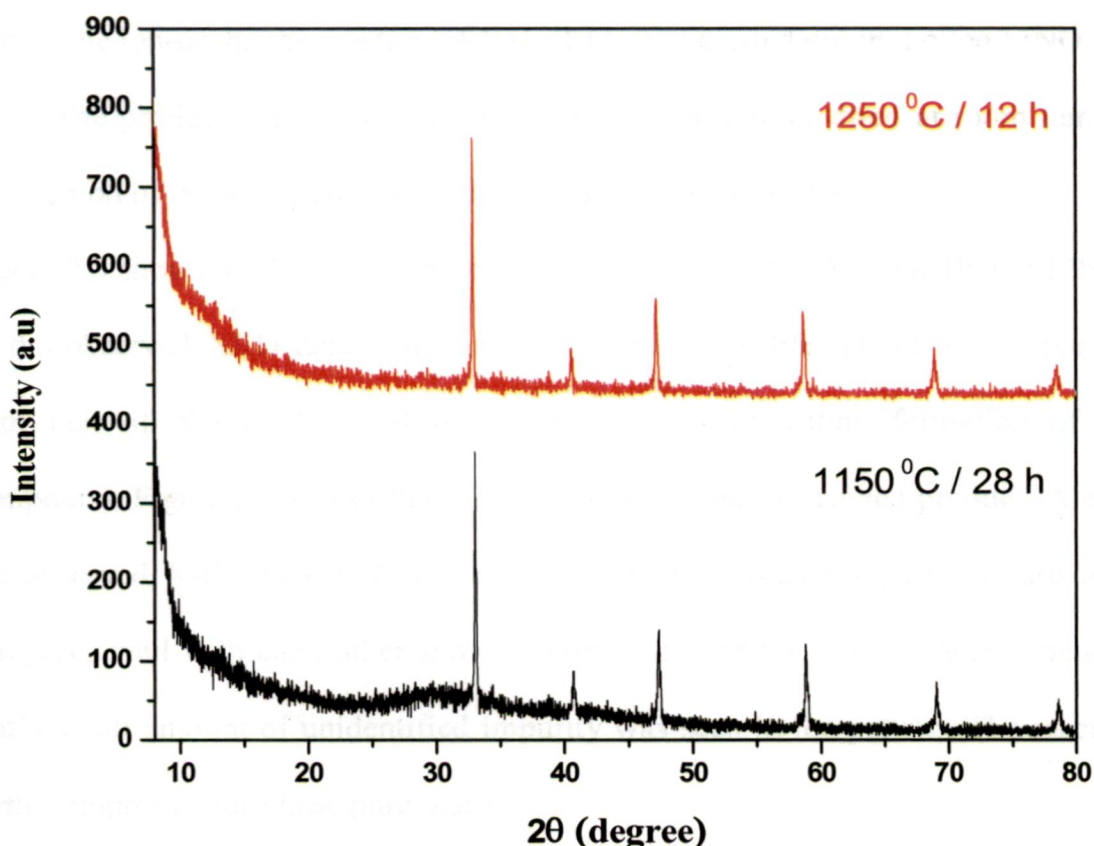


**Figure 2.2** Powder XRD patterns of nominal  $\text{Li}_{0.10}\text{Ca}_{0.35}\text{La}_{0.40}\text{TiO}_3$  at two different temperatures.



Comparison of the observed XRD data compares excellently with the literature data for the compound,  $\text{Li}_{0.5}\text{La}_{0.5}\text{TiO}_3$  (64).

### 2.3 Synthesis and Characterization of $\text{LiLaTiO}_4$

The  $\text{LiLaTiO}_4$  was synthesized by a ion exchange of a parent compound  $\text{NaLaTiO}_4$ ,  $\text{NaLaTiO}_4$  was synthesized by a conventional solid state reaction.(29) The starting materials were a mixture of sodium carbonate, rare earth oxide ( $\text{La}_2\text{O}_3$ ) and titanium oxide ( $\text{TiO}_3$ ). The raw material  $\text{La}_2\text{O}_3$  (99.99%) of from CDH analytical reagent,  $\text{Na}_2\text{CO}_3$  of (99.99%) from SRL, and  $\text{TiO}_2$  (99.99%) of CDH analytical reagent were used. An excess amount of sodium carbonate  $\sim 30$  mol% was added to compensate for the loss due to the evaporation of the sodium component at higher temperatures. The mixture was fired for 12 hr at 900–1000 °C in air. The ion-exchange reaction of  $\text{NaLaTiO}_4$  was carried out in molten  $\text{LiNO}_3$  at 300 °C for 12 h. The product was washed with distilled water and air dried at room temperature. The completion of the ion-exchange reaction was confirmed by XRD.

Figure 2.3 shows the XRD pattern of  $\text{NaLaTiO}_4$  heated at 950 °C for 1h and 12h. Comparison of the observed XRD data with the reported database files (JCPDS) compares excellently with that of  $\text{NaLaTiO}_4$  (card no. # 86-0828) is indicating formation of single phase compound. Figure 2.4 shows that XRD data of the ion-exchanged product. A comparison of the observed XRD data with the reported data for  $\text{LiLaTiO}_4$  (JCPDS card no. #89-0379) compares well with each other showing completion of the ion exchange reaction, excepting that a small amount of unidentified impurity was seen in the pattern. The reaction has to be further improved for phase pure materials.

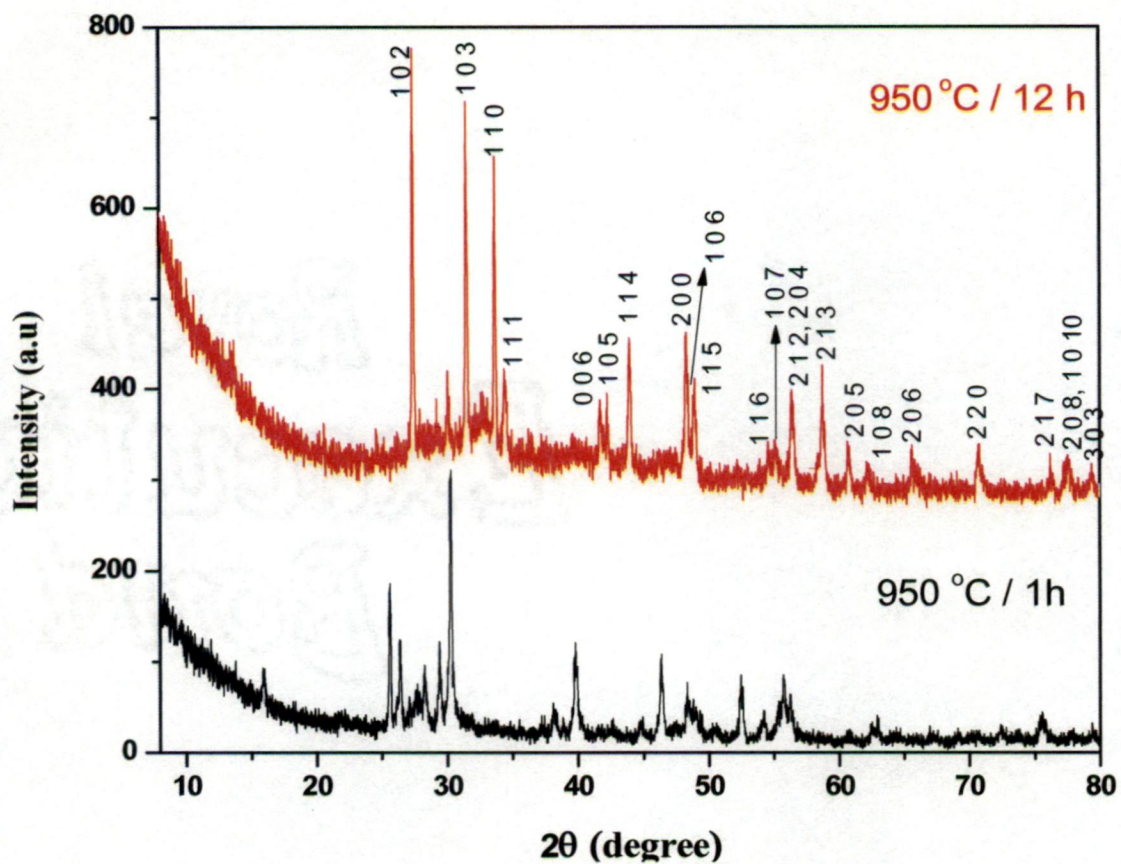


Figure 2.3 Powder XRD pattern of NaLaTiO<sub>4</sub> heated at 950 °C for 1 h and 12 h.

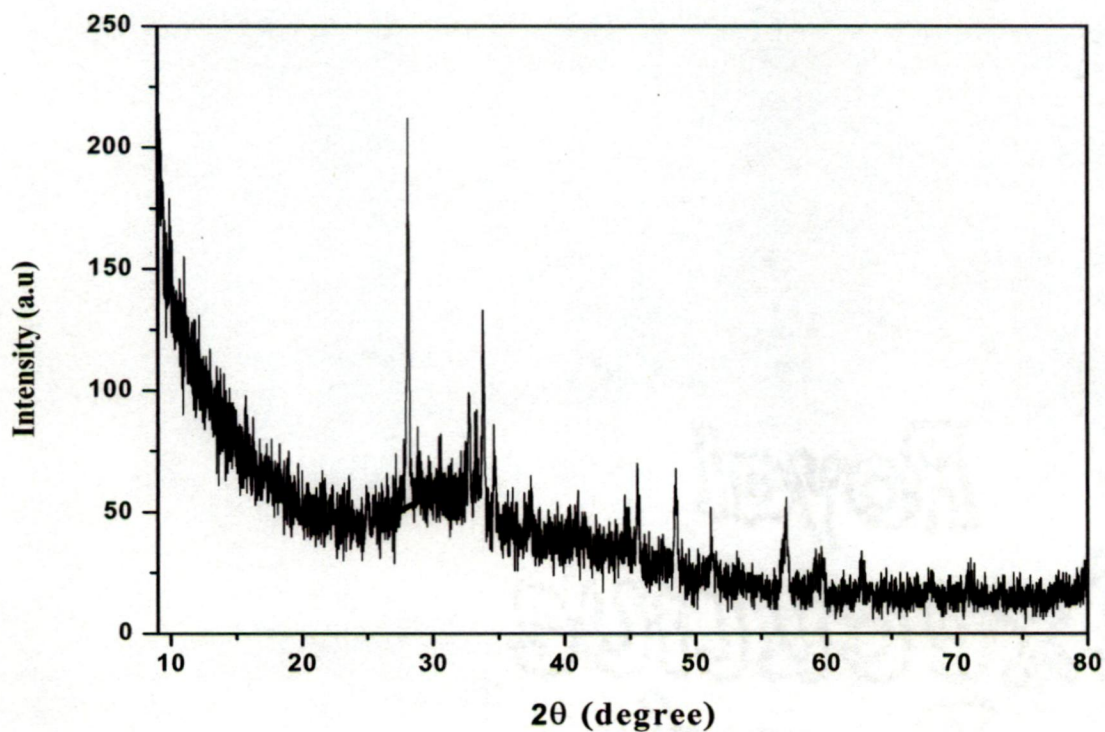


Figure 2.4 Powder XRD pattern of LiLaTiO<sub>4</sub>.

## 2.4 Synthesis and characterization of $\text{Li}_2\text{La}_2\text{Ti}_3\text{O}_{10}$

The  $\text{Li}_2\text{La}_2\text{Ti}_3\text{O}_{10}$  was synthesized by a conventional solid state reaction directly. The starting materials were a mixture of lithium carbonate ( $\text{Li}_2\text{CO}_3$ ), lanthanum oxide ( $\text{La}_2\text{O}_3$ ) and titanium dioxide ( $\text{TiO}_2$ ). The raw materials  $\text{La}_2\text{O}_3$  (99.99%) from CDH analytical reagent,  $\text{Li}_2\text{CO}_3$  (99.99%) from Sigma Aldrich, and  $\text{TiO}_2$  (99.99%) from CDH analytical reagent were used. An excess amount of lithium carbonate (~30 mol%) was added to compensate for the loss due to the evaporation of the lithium component. The mixture was initially heated at 550 °C for 12 h and subsequently the temperature was progressively raised reaching 1100 °C in the final stage. Figure 2.5 shows the powder XRD pattern of  $\text{Li}_2\text{La}_2\text{Ti}_3\text{O}_{10}$  obtained at 1100 °C.

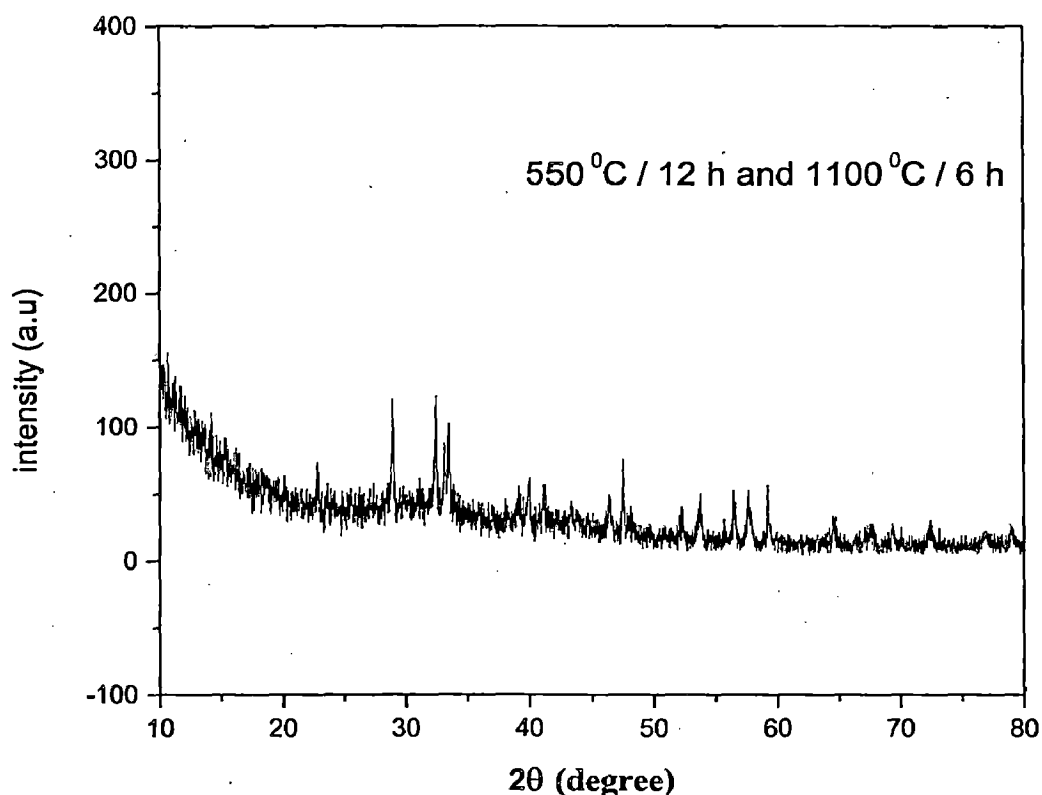


Figure 2.5 Powder XRD pattern of  $\text{Li}_2\text{La}_2\text{Ti}_3\text{O}_{10}$  obtained at 1100 °C.

Comparison of the observed XRD data of  $\text{Li}_2\text{La}_2\text{Ti}_3\text{O}_{10}$  with the reported database files (JCPDS) indicates formation of  $\text{Li}_2\text{La}_2\text{Ti}_3\text{O}_{10}$  (card no. # 87-1169). However, formation of considerable amount of  $\text{LaTiO}_3$  (JCPDS card no. # 34-0596) as an impurity phase could not be avoided under this synthetic condition. Further work is necessary to improve upon the synthesis to obtain phase pure compounds.

## 2.5 X-ray diffraction simulation and lattice parameter refinement of $\text{Li}_{0.10}\text{Ca}_{0.35}\text{La}_{0.40}\text{TiO}_3$

Based on our structural database (JCPDS files) search we realized that the compound  $\text{Li}_{0.10}\text{Ca}_{0.35}\text{La}_{0.40}\text{TiO}_3$  stabilizes in a hexagonal structure similar to that adopted by  $\text{Li}_{0.5}\text{La}_{0.5}\text{TiO}_3$ . The structure of  $\text{Li}_{0.5}\text{La}_{0.5}\text{TiO}_3$  is described by a network of  $\text{TiO}_6$  octahedra which is slightly tilted the pseudocubic rhombohedral axes in order to optimize the La-O distances (64). The La positions are 12 coordinated and half occupied in a random manner, leaving half the site vacant per formula unit. The  $\text{Li}^+$  cations are four coordinated to oxygen in square planer coordination. In other words, they are placed in the window formed by four  $\text{TiO}_6$  corner connected octahedra as shown in Figure 2.6.

Realizing the close similarity of observed diffraction pattern to that of  $\text{Li}_{0.5}\text{La}_{0.5}\text{TiO}_3$ , we have constructed a model structure similar to  $\text{Li}_{0.5}\text{La}_{0.5}\text{TiO}_3$  for our compound, where we have placed Ca in the remaining La position while Li position remains the same. We have also adjusted the  $x$  parameter of the oxygen by taking into consideration that the  $c$ -parameter of our compound is slightly smaller than that of  $\text{Li}_{0.5}\text{La}_{0.5}\text{TiO}_3$ . The thermal parameters for our compound were taken from the model compound. The occupancies were adjusted according to our composition. Table 2.1 shows the lattice parameters and positional parameters as used in the simulation.

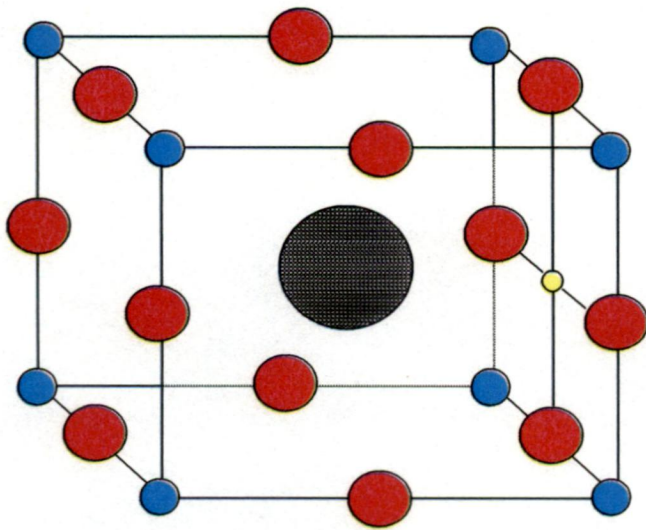


**Figure 2.6** Schematic structure of  $\text{Li}_{0.5}\text{La}_{0.5}\text{TiO}_3$  showing the location of La (big grey sphere at the centre) and Li (yellow small sphere at the face centre). Oxygen is shown by red spheres and the Ti is shown in blue spheres.

**Table 2.1** The atom positional parameters, occupancies and thermal parameters for  $\text{Li}_{0.15}\text{Ca}_{0.35}\text{La}_{0.40}\text{TiO}_3$  as used in the simulation.\*

Atom	Site	X	y	z	$f_{\text{occ}}$	$B_{\text{iso}} (\text{\AA}^2)$
La	6a	0	0	0.25	0.40	0.17
Ca	6a	0	0	0.25	0.35	0.17
Li	18d	0.5	0	0	0.15	6.7
Ti	6b	0	0	0	1.0	1.17
O	18e	0.5346	0	0.25	1.0	1.75

\* Cell parameters:  $a = 5.444 \text{ \AA}$ ,  $c = 13.34 \text{ \AA}$ ,  $\alpha = 90^\circ$ ,  $\beta = 90^\circ$  and  $\gamma = 120^\circ$ .

The observed XRD pattern of  $\text{Li}_{0.15}\text{Ca}_{0.35}\text{La}_{0.40}\text{TiO}_3$  and the simulated patterns of both  $\text{Li}_{0.15}\text{Ca}_{0.35}\text{La}_{0.40}\text{TiO}_3$  and  $\text{Li}_{0.5}\text{La}_{0.5}\text{TiO}_3$  are shown in Figure 2.6. The exact peak positions

and intensity ratios of the simulated data of  $\text{Li}_{0.15}\text{Ca}_{0.35}\text{La}_{0.40}\text{TiO}_3$  with that of the observed data confirms the structural model of our compound.

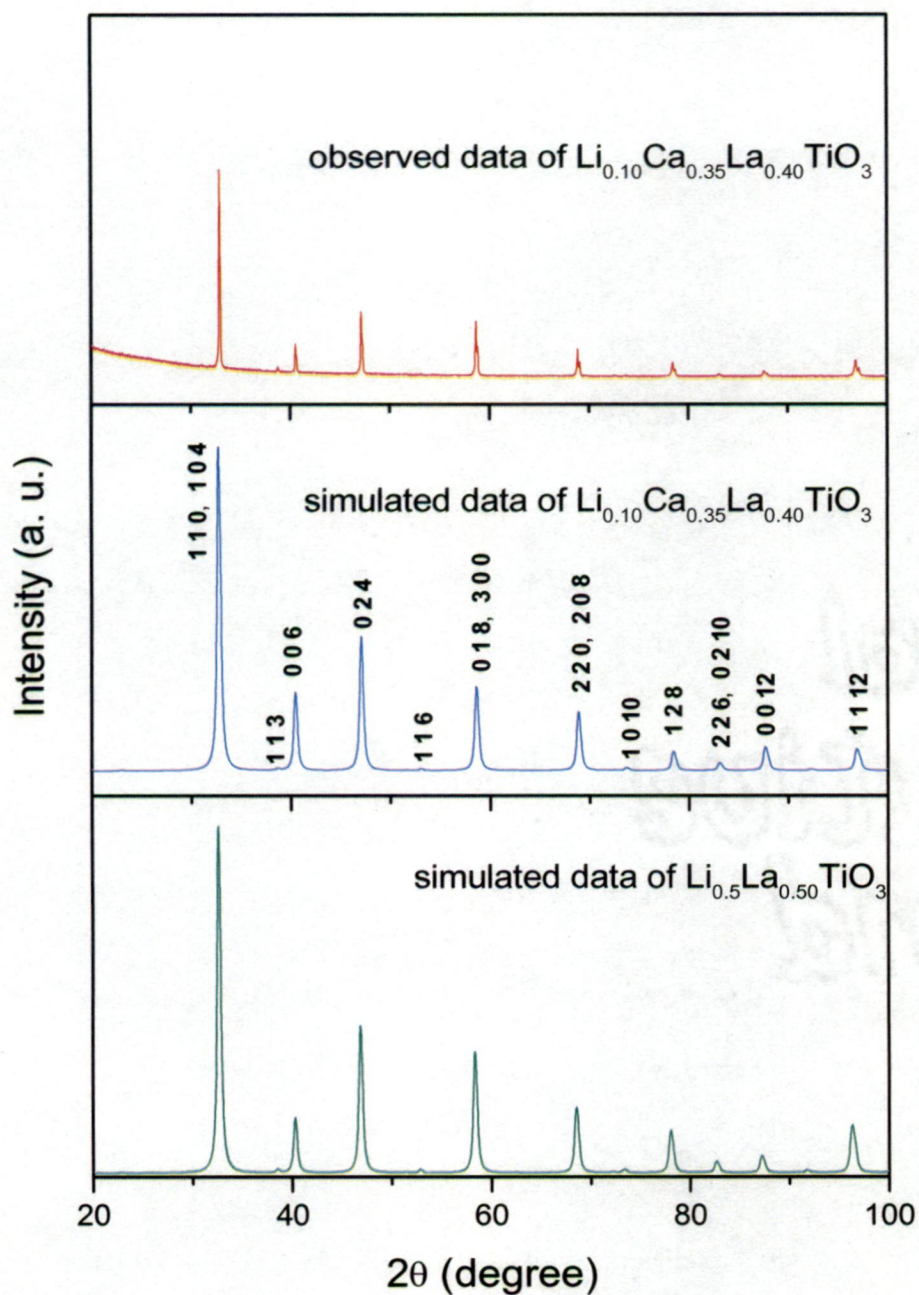


**Figure 2.6** Observed (top) and simulated (middle) XRD patterns of  $\text{Li}_{0.15}\text{Ca}_{0.35}\text{La}_{0.40}\text{TiO}_3$  based on a model structure of  $\text{Li}_{0.5}\text{La}_{0.5}\text{TiO}_3$ . The bottom pattern is the simulated XRD profile based on its crystallographic data (64).

## Chapter-3

### Compositional Analysis by FE-SEM and EDAX

The crystallite & morphology and chemical compositional analysis are carried out by FE-SEM & EDAX analysis respectively. For this analysis we prepared some compounds of Lithium Lanthanum Titanate series, out of these compounds some are analysed by XRD pattern and some are analysed by XRD as well as SEM-EDAX.

#### Sample preparation for FE-SEM & EDAX

For this purpose a small amount of sample ~ 5-10 mg was put on a carbon tape pasted on a stainless steel stub. Since our samples were electronically non-conducting, a conductive coating of gold was required for the sample to be analysed under FE-SEM. The gold coating was carried out in a sputtering unit. In conventional SEM sputter coating a gold (gold-palladium, or platinum) target is bombarded with heavy gas atoms (argon). Metal atoms ejected from the target by the ionized gas cross the plasma to deposit onto the any surface within the coating unit including the specimen. A low vacuum environment is used ~ 0.1 to 0.05 mbar, with one of the modern low voltage sputter coaters that enables metal to be deposited at up to 1 nm / s. Sputtered metals are deposited in the form of islands, not a continuous coating. This coating will be relatively random not in a uniform manner.

The SEM images are taken using Quanta 200 F, FEI Netherland instrument. The images are taken at working distance (WD) 10.5 mm, operating voltage of 20 kV and at magnification of 2000, 8000, 15000, and 32000.

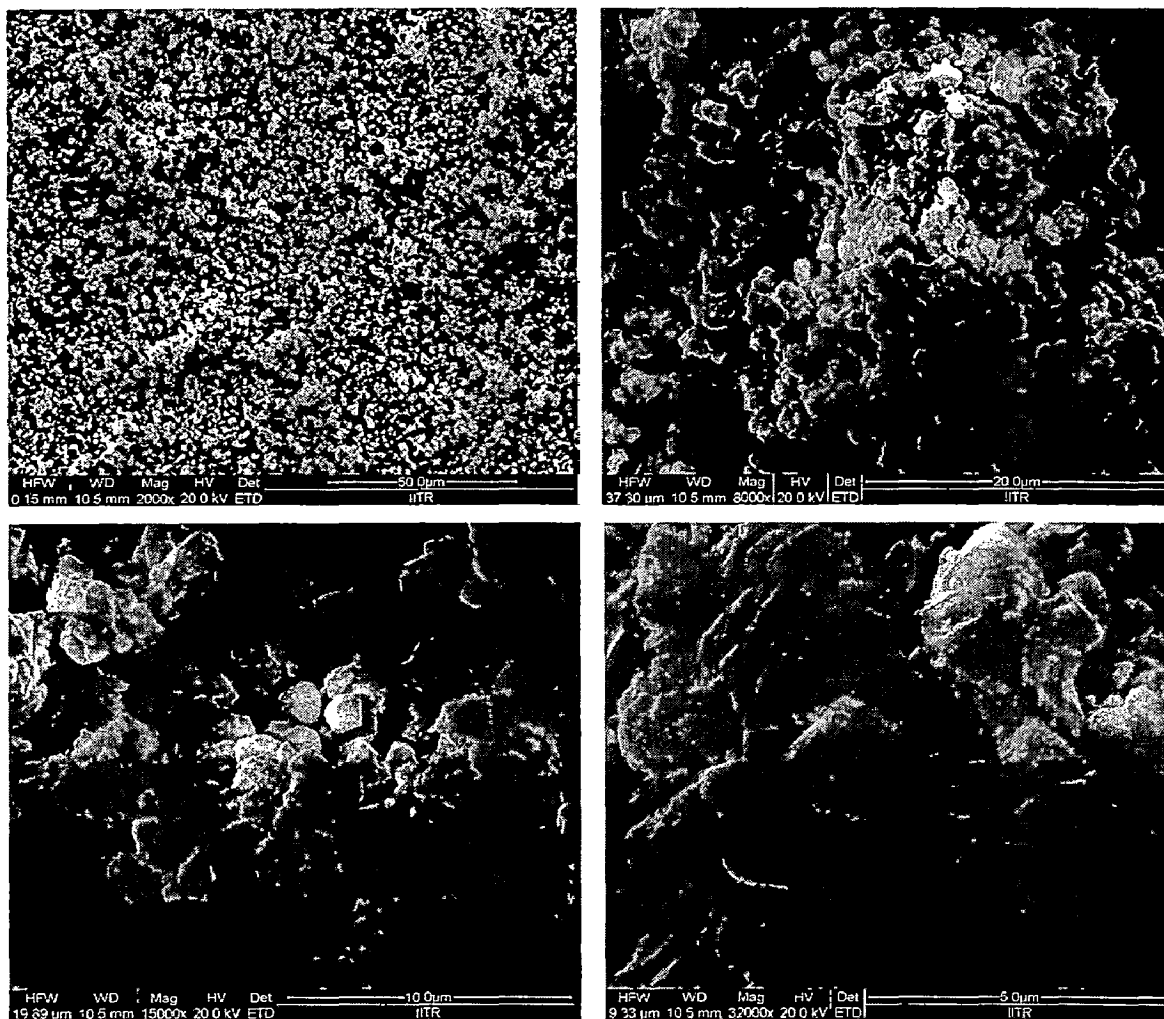
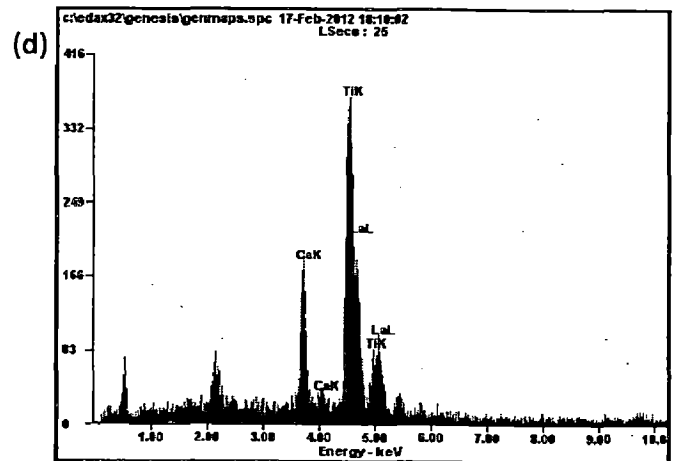
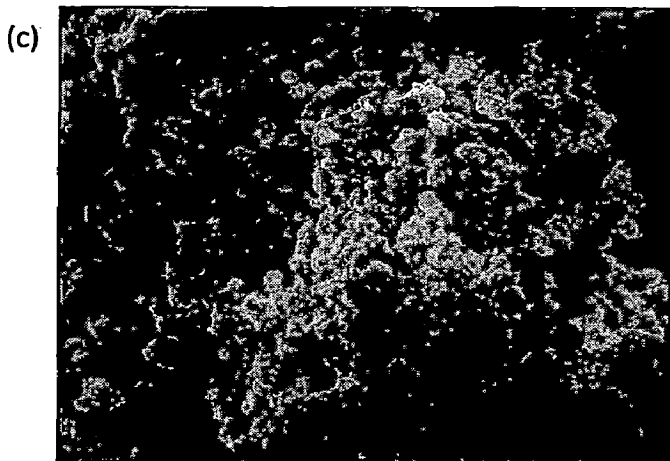
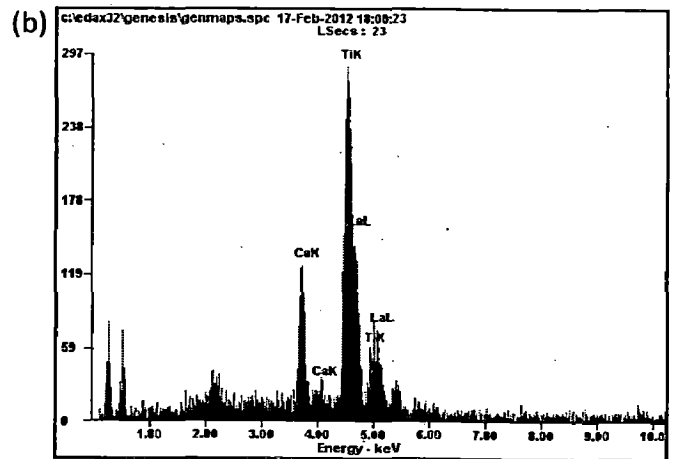
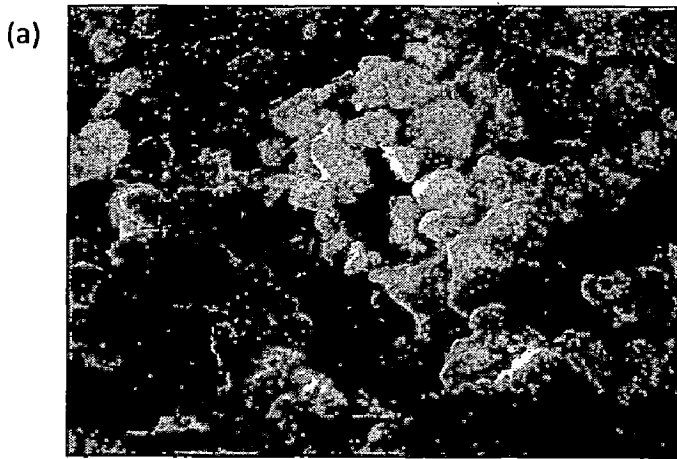


**Figure 3.1** SEM images of the as synthesized  $\text{Li}_{0.10}\text{Ca}_{0.35}\text{La}_{0.40}\text{TiO}_3$  showing morphological uniformity throughout the sample at different magnifications (a) at 2000 $\times$  (b) 8000 $\times$  (c) 15000 $\times$  (d) 32000 $\times$ .



The particle morphologies look homogeneous. For calculating the composition of the compound, we have scanned various regions in our sample. In a particular region, we have selected several crystallites and carried out the EDAX (point basis) to find out the composition. Figure 3.2 shows the SEM images, EDX spectra and elemental percentages of  $\text{Li}_{0.10}\text{Ca}_{0.35}\text{La}_{0.40}\text{TiO}_3$ . In figure 3.2, (a) and (c) are the SEM image showing the spots (+ symbols) & (b) and (d) show the corresponding EDX spectra confirming the presence of Ca, Ti and La. Panels (e) and (f) at the bottom show the corresponding elemental percentages. The elemental composition was uniform throughout the sample as observed in the EDAX spectra at various regions and spots (crystallites). The SEM-EDX data is in conformity with the powder XRD investigation wherein we have confirmed the single phase nature by simulation of XRD data on a structural model based on  $\text{Li}_{0.10}\text{Ca}_{0.35}\text{La}_{0.40}\text{TiO}_3$ .

Figure 3.3 shows SEM images of  $\text{Li}_{0.16}\text{La}_{0.62}\text{TiO}_3$  the as synthesized samples showing morphology of sample at different magnifications (a) at 2000× (b) 4000× (C) 8000× (d) 16000×. Although the particle morphologies look quite homogeneous but the EDX spectra and elemental composition (Figure 3.4) signifies local inhomogeneity with slight variation of elemental percentages of La and Ti. This could have resulted due to local fluctuations in the composition of Li in the sample during grinding. However, the XRD analysis showed quite satisfactory result in terms of its single phase nature. Therefore, careful synthesis is required to have compositionally good homogeneous samples.



(e)

Element	Wt%	At%
CaK	10.95	18.97
TiK	38.46	55.74
LaL	50.59	25.29
Matrix	Correction	ZAF

(f)

Element	Wt%	At%
CaK	10.91	18.78
TiK	39.21	56.46
LaL	49.87	24.76
Matrix	Correction	ZAF

Figure 3.2 (a) and (c) are the SEM image showing the spots (+ symbols) and (b) and (d) show the corresponding EDX spectra confirming the presence of Ca, Ti and La. Panels (e) and (f) at the bottom show the corresponding elemental percentages.

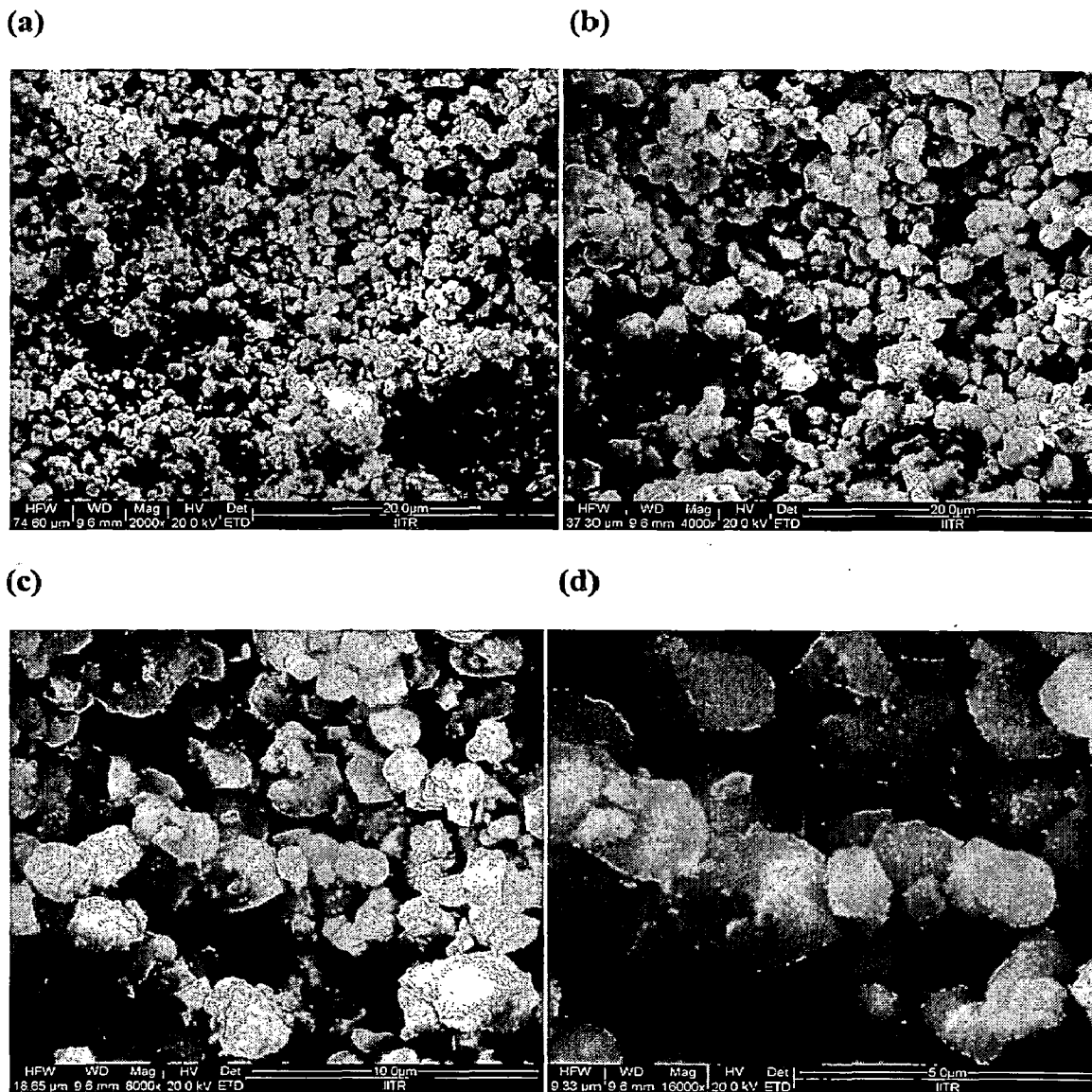
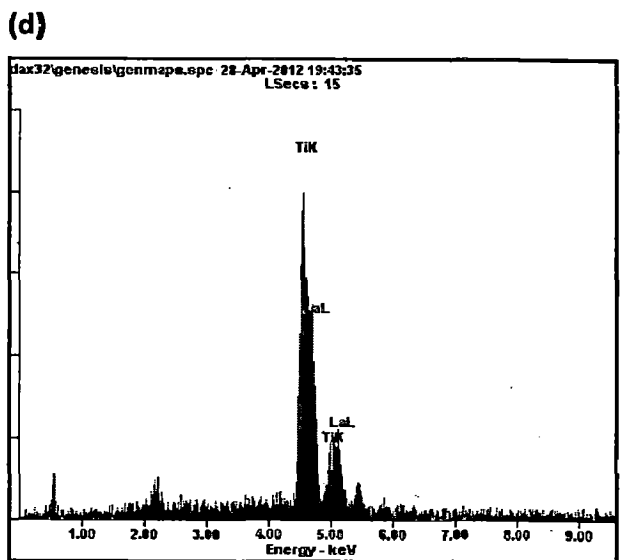
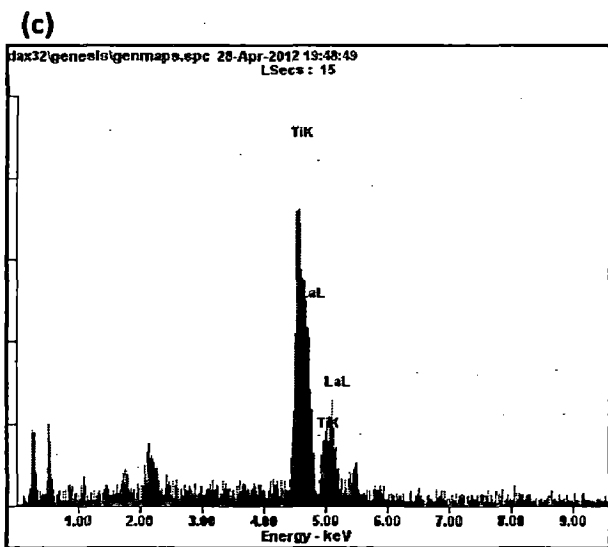
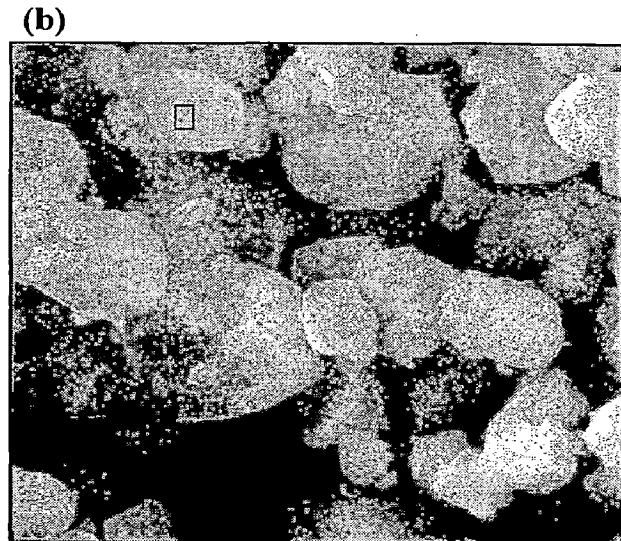
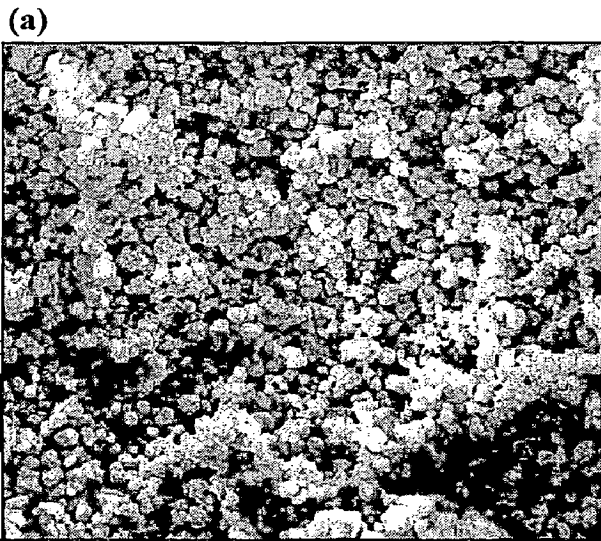


**Figure 3.3** SEM images of  $\text{Li}_{0.16}\text{La}_{0.62}\text{TiO}_3$  the as synthesized showing morphology of sample at different magnifications (a) at 2000× (b) 4000× (c) 8000× (d) 16000×.



(e)

Element	Wt%	At%
<i>TiK</i>	37.79	63.79
<i>LaL</i>	62.21	36.21
<i>Matrix</i>	Correction	ZAF

(f)

Element	Wt%	At%
<i>TiK</i>	35.55	61.53
<i>LaL</i>	64.45	38.47
<i>Matrix</i>	Correction	ZAF

Figure 3.4 (a) and (b) are the SEM images & (c) and (d) show the corresponding EDX spectra confirming the presence of Ca, Ti and La. Panels (e) and (f) at the bottom show the corresponding elemental percentages.

## Chapter-4

### <sup>6</sup>Li, <sup>7</sup>Li and MAS-NMR investigation of 2D and 3D Oxides

Solid state NMR has emerged as an extremely useful tool for characterizing the local structure of Li-ion conducting materials. The lithium ions naturally occur in two isotopic forms, <sup>7</sup>Li and <sup>6</sup>Li with <sup>7</sup>Li being the highly abundant one (<sup>7</sup>Li: 92.58%; <sup>6</sup>Li: 7.42%). Therefore, <sup>6</sup>Li and <sup>7</sup>Li are directly involved in the electrochemical processes and they can be used as probe to investigate the changes that occur locally in the material. The <sup>6</sup>Li and <sup>7</sup>Li spectra are strongly influenced by electronic environment of Li ion. The NMR method is quantitative and can be used to determine which species are removed on charging the battery and how the local structure changes. NMR is also sensitive to dynamics, so 1-D and 2-D NMR have been used to investigate the Li ion motion. The motion of Li ions plays not only an important role in liquid and solid electrolytes, but also in metals and electrode materials for which there is both electron and ion conduction.

From the NMR point of view, it is fortunate that Li has two stable isotopes, <sup>6</sup>Li and <sup>7</sup>Li. Due to the differences in the nuclear properties, such as the magnitudes of the magnetic dipole and electrical quadrupole moments, the <sup>6</sup>Li and <sup>7</sup>Li species can provide two different views of the structure and dynamics of ion conductors. Besides being quadrupolar in nature as they possess spin number which is greater than ½, the two nuclei by themselves differ in the NMR spectral response as compared to spin ½ systems. For <sup>6</sup>Li which has spin 1, first-order quadrupolar effects alone matter as <sup>6</sup>Li is amenable for magic angle spinning due to the favourable averaging of the quadrupolar broadening at the 'magic angle' ( $\cos^{-1}1/\sqrt{3} = 54.736^\circ$ ) due to the  $P_2\cos(\theta)$  orientation dependence in a powder sample. This can be

contrasted to the  $^7\text{Li}$  case for which the spin number is  $3/2$ . Second-order quadrupole effects become important in the case of  $^7\text{Li}$  (spin number  $3/2$ ) and it is also recognized that magic angle spinning (MAS) is of no avail in the case of half-integer quadrupolar spins as the second-order quadrupolar broadening is governed by both  $P_2\cos(\theta)$  and  $P_4\cos(\theta)$  terms. Although Multiple Quantum Magic Angle Spinning (MQ MAS) technique can be effectively employed in the case of half-integer quadrupolar nuclei,  $^7\text{Li}$  is more favourably disposed for MAS studies due to the smaller values of its quadrupole coupling in molecular crystals. In spite of the increased quadrupolar interaction of  $^7\text{Li}$  over  $^6\text{Li}$ ,  $^7\text{Li}$  is inherently more sensitive due to its very high abundance. For structural analysis, there are several reviews on the NMR methods (65–71) in which magic angle spinning (MAS) techniques are involved. When dynamical aspects are in the focus of interest the role of MAS is less prominent, but the analyses of line-shapes and spin-relaxation times continue to provide valuable sources of information on Li ion conductors given in the ref. (72).

#### 4.1 Experimental

Solid state NMR experiments were performed at the superconducting magnetic field strength of 9.4 Tesla on a Bruker DRX-400 NMR spectrometer. The Larmor frequencies for  $^6\text{Li}$  and  $^7\text{Li}$  were 58.864 and 155.452 MHz, respectively. The experiments were conducted in the static and magic angle spinning modes. Magic angle was precisely set using KBr sample and monitoring the ‘satellite transitions’ and optimizing the ‘rotational echoes’. Free inductions were acquired in the Bloch decay mode using a ‘zg’ single pulse sequence. A flip angle of  $10\text{--}15^\circ$  was used for the excitation pulse with a 2–4 sec recycle delay. Typically 4000 and 800 transients were acquired for the static and MAS measurements, respectively, and the time averaged signal was Fourier transformed after apodization using an exponential function with

a line broadening of 10-100 Hz. In the case of MAS, two experiments were performed at different spinning speeds to clearly identify the centre peaks and their associated spinning side bands.

#### 4.2 $^6\text{Li}$ , $^7\text{Li}$ and MAS-NMR studies of $\text{Li}_{0.10}\text{Ca}_{0.35}\text{La}_{0.40}\text{TiO}_3$

Solid state lithium NMR spectra recorded for nominal  $\text{Li}_{0.10}\text{Ca}_{0.35}\text{La}_{0.40}\text{TiO}_3$  are presented in Figures 4.1, 4.2 and 4.3 for  $^6\text{Li}$  and  $^7\text{Li}$  (static and MAS) measurements, respectively. No information about the multiplicity of lithium environments is provided from  $^6\text{Li}$  spectra. On the other hand,  $^7\text{Li}$  spectra clearly reveal the presence of two non-equivalent lithium sites, (I & II) which are marked as 1 and 2 in the figure. The two sites are distinguished based on the difference in their chemical shifts. Of these, site I is more intense and additionally exhibits a large number of spinning side bands. By comparison, site II is less intense and this site depicts less number of spinning side bands. To a first degree, the observed integrated intensities reflect the population of the two sites in the structure.

As the spinning side bands originate from the first-order averaging of the 'satellite transitions' ( $\pm 1/2 \leftrightarrow \pm 3/2$ ), the observed manifold of spinning side bands is a measure of the  $^7\text{Li}$  electric field gradient (EFG) that is getting averaged by MAS. That the spinning side band manifold for site I is much intense and occurs over a much larger frequency spread is an indication that site I suffers a larger perturbation to the EFG as compared to site II.

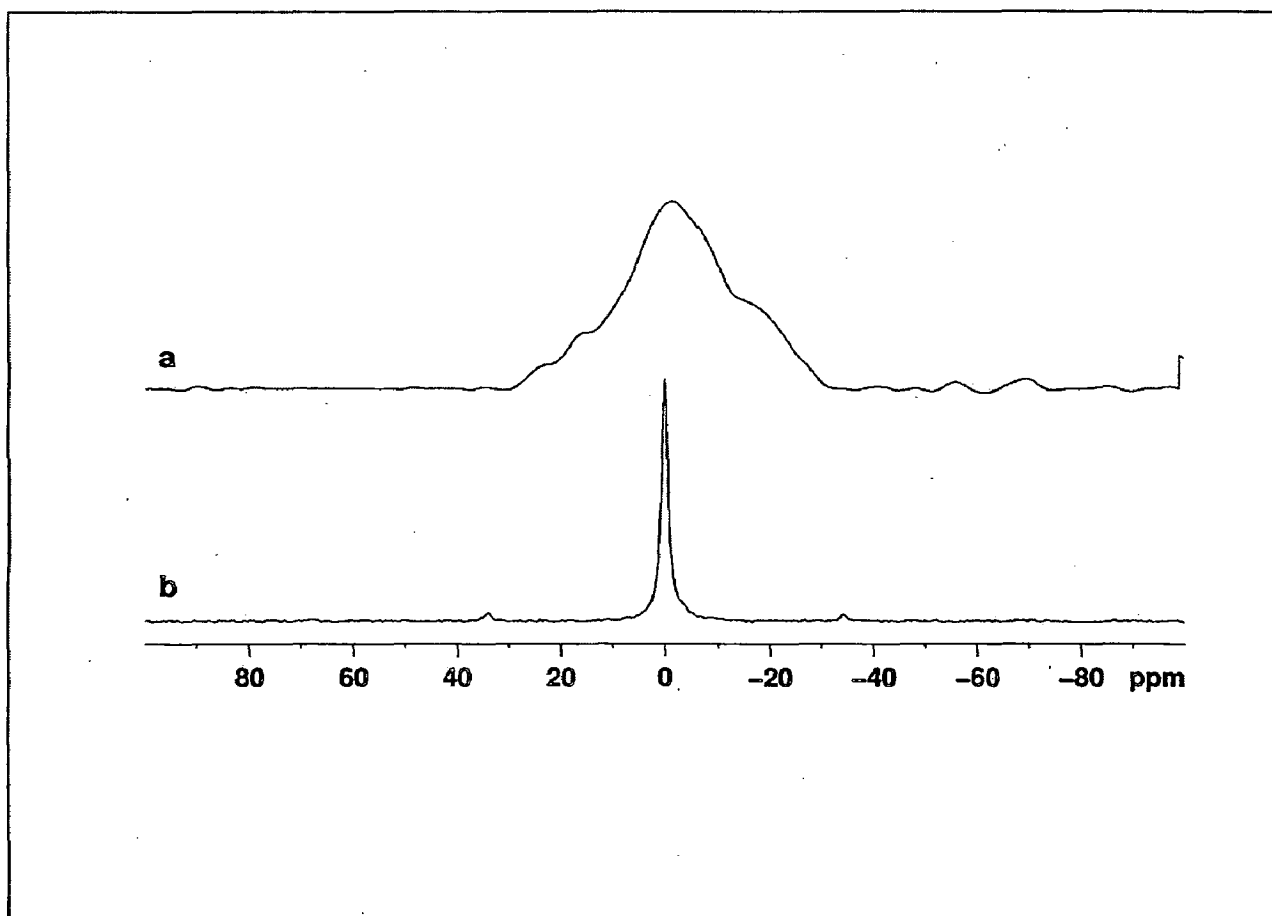


Figure 4.1  ${}^6\text{Li}$  NMR spectra of  $\text{Li}_{0.10}\text{Ca}_{0.35}\text{La}_{0.40}\text{TiO}_3$ .

Overall, the solid state  ${}^7\text{Li}$ <sup>NMR</sup> results indicate that the geometrical distortion at site I is much greater, whereas for site II the distortion is much smaller by comparison. It may be noted that these insights are provided by  ${}^7\text{Li}$  spectra and are missing in the  ${}^6\text{Li}$  spectra. This is due to the smaller quadrupolar effects seen in the case  ${}^6\text{Li}$  and is attributable to the smaller value of the quadrupole moment ( $eQ = -0.08$ ). The quadrupolar effects are amplified in the  ${}^7\text{Li}$  MAS spectra due to its larger quadrupole moment ( $eQ = -4.01$ ) and this has made the site distinction possible by  ${}^7\text{Li}$  MAS NMR.



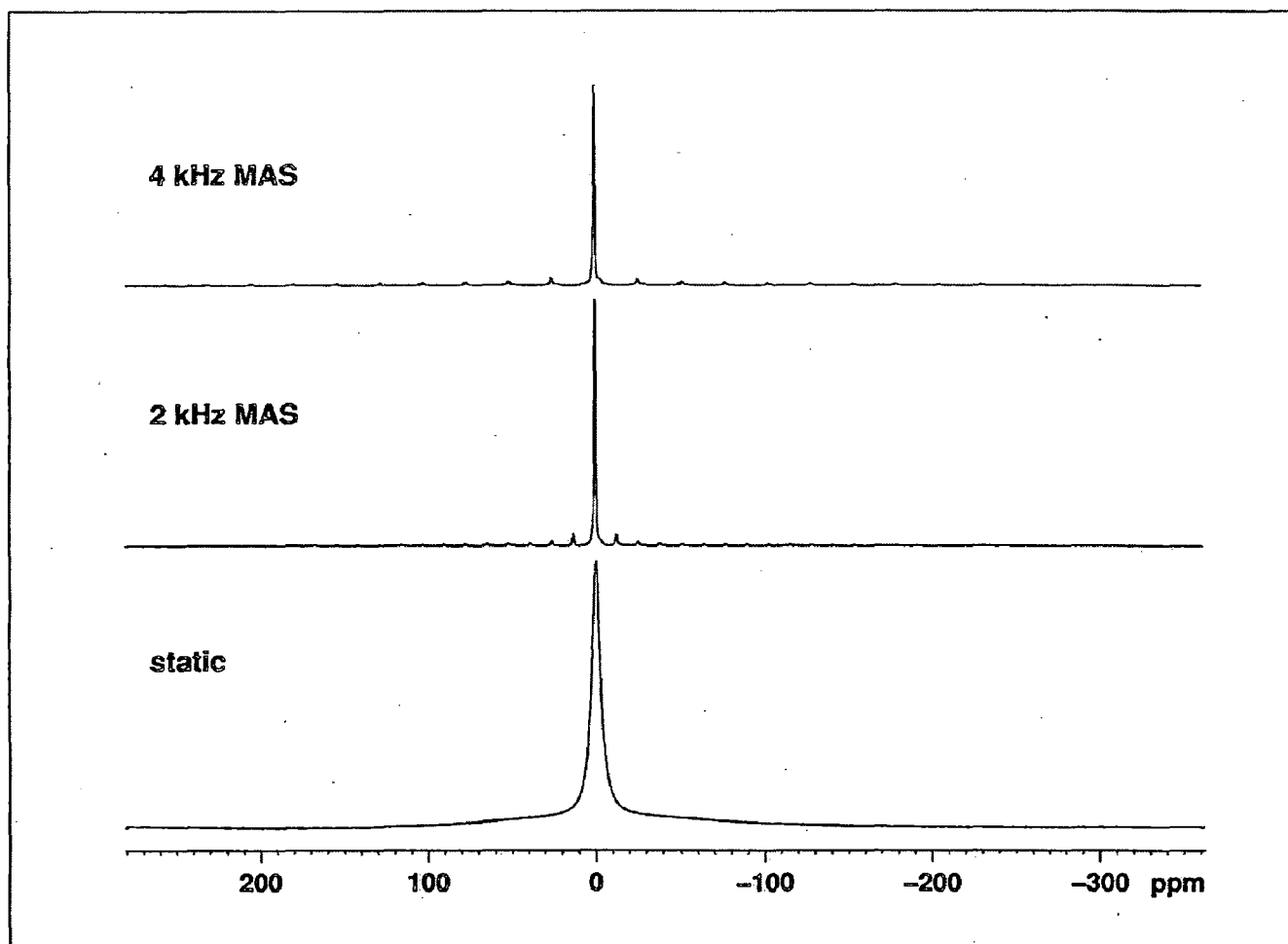
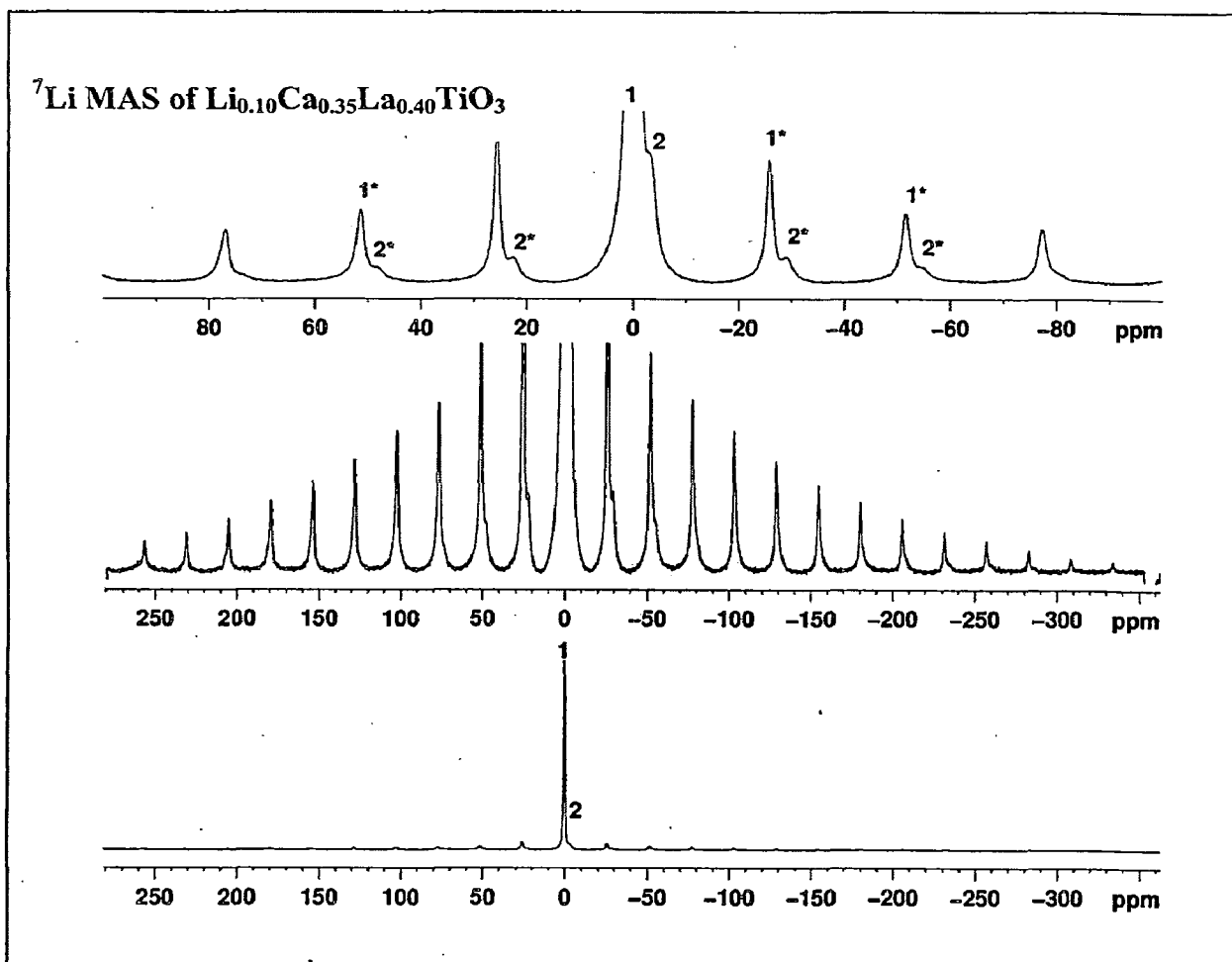


Figure 4.2  ${}^7\text{Li}$  NMR spectra of  $\text{Li}_{0.10}\text{Ca}_{0.35}\text{La}_{0.40}\text{TiO}_3$ .



**Figure 4.3**  ${}^7\text{Li}$  MAS-NMR spectra of  $\text{Li}_{0.10}\text{Ca}_{0.35}\text{La}_{0.40}\text{TiO}_3$ .

At this juncture, a comment on the possibility of two Li-sites, which is in contradiction to our structural model used in the XRD simulation, is in place. The  ${}^7\text{Li}$ -MAS NMR clearly indicated two Li sites; one is symmetrical while the other is in a distorted coordination environment. According to our structural model, the more symmetrical site will be the one where Li is in pseudo square planer coordination (II) in this compound. However, within this model some amount of Li sitting in the unsymmetrical site could not be completely ruled out based on the XRD data. Because, La and Ca are located at the A-site where 25% sites are still vacant and if Li has to sit at this site it would adopt a highly unsymmetrical coordination and

hence experiencing higher electric field gradient. However, this requires reinvestigation to ascertain if such a distribution of Li is actually happening in the material.

#### 4.3 ${}^6\text{Li}$ , ${}^7\text{Li}$ and MAS-NMR studies of $\text{Li}_{0.16}\text{La}_{0.62}\text{TiO}_3$

Solid state lithium NMR spectra recorded for nominal  $\text{Li}_{0.16}\text{La}_{0.62}\text{TiO}_3$  are presented in Figures 4.4 – 4.6, for  ${}^6\text{Li}$  and  ${}^7\text{Li}$  (static and MAS) measurements. Figure 4.4 shows the  ${}^6\text{Li}$  static and MAS-NMR spectra of  $\text{Li}_{0.16}\text{La}_{0.62}\text{TiO}_3$ . In this compound, both the static and MAS NMR data clearly indicates presence of two different lithium sites. On the other hand, in  ${}^7\text{Li}$  both the static (Figure 4.5a) and small field MAS (Figure 4.5b) spectra cannot resolve the two Li-sites due to strong quadrupolar interaction. However, at higher field strengths the two distinct sites start to resolve (Figure 4.5c & 4.5d). Figure 4.6 shows the resolution enhanced  ${}^{6,7}\text{Li}$  MAS-NMR spectra at 5 kHz of  $\text{Li}_{0.16}\text{La}_{0.62}\text{TiO}_3$ . The expanded central signal clearly indicates two sites with a distribution  $\sim 2:1$  among the sites. The sharp peak could be assigned to the more mobile lithium at room temperature, since the higher mobility will result in motional narrowing of the line width. A comparison of the  ${}^7\text{Li}$  MAS NMR spectra of  $\text{Li}_{0.10}\text{Ca}_{0.35}\text{La}_{0.40}\text{TiO}_3$  and  $\text{Li}_{0.16}\text{La}_{0.62}\text{TiO}_3$  indicated that while split side bands are present in the former, in the later the side bands are more symmetric. This could possibly indicate that the Ca-analogue will show a reduced Li-ion mobility, hence smaller bulk conductivity as compared to  $\text{Li}_{0.16}\text{La}_{0.62}\text{TiO}_3$ .

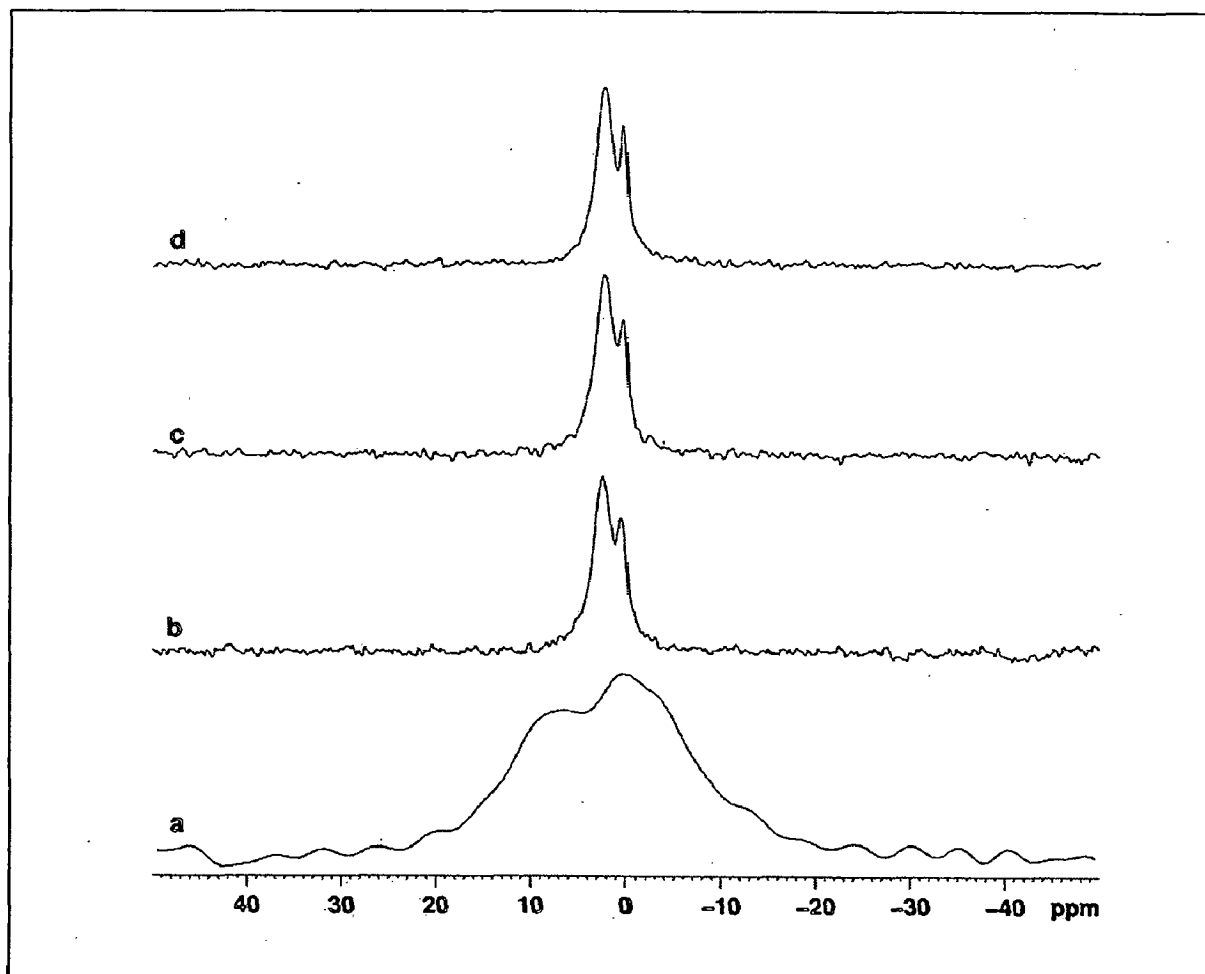


Figure 4.4  ${}^6\text{Li}$  static (a) and MAS (b-d) NMR spectra of  $\text{Li}_{0.16}\text{La}_{0.62}\text{TiO}_3$ .

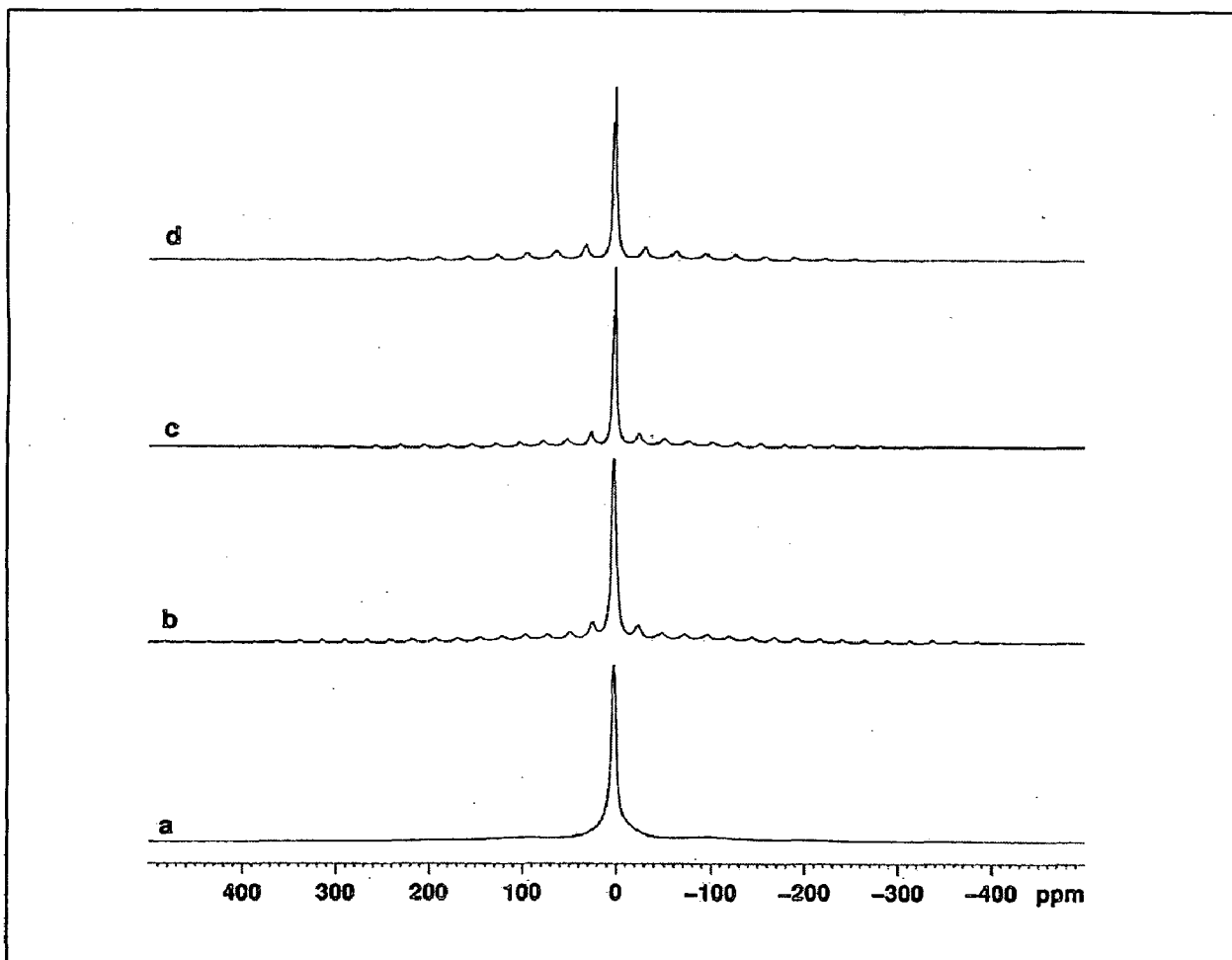


Figure 4.5  ${}^7\text{Li}$  MAS-NMR spectra of  $\text{Li}_{0.16}\text{La}_{0.62}\text{TiO}_3$ .

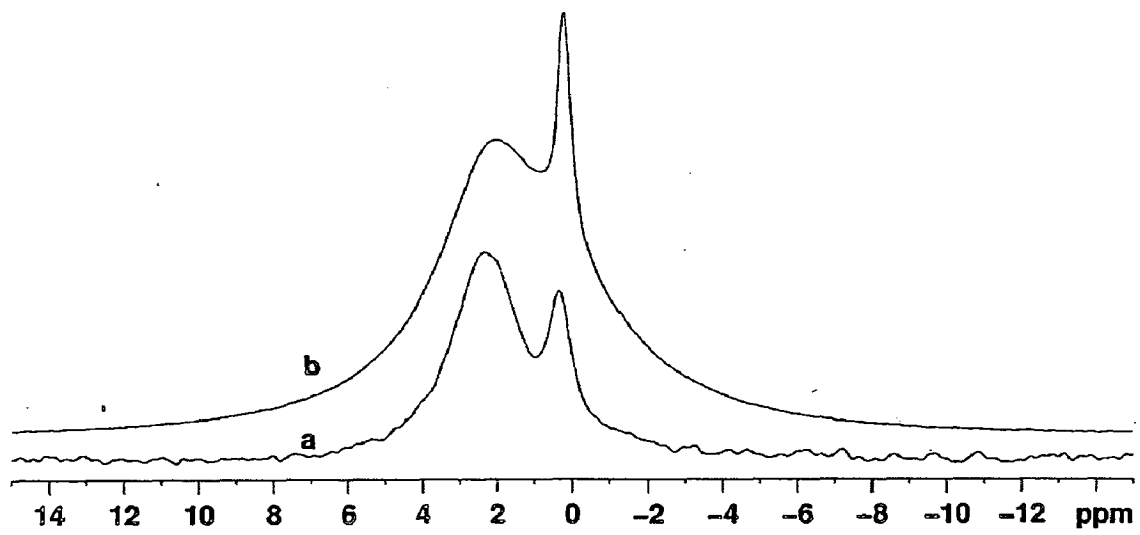


Figure 4.6 Resolution enhanced  $^{6,7}\text{Li}$  MAS-NMR spectra at 5 kHz of  $\text{Li}_{0.16}\text{La}_{0.62}\text{TiO}_3$ .

## Conclusion

We have synthesized lithium, calcium, lanthanum and titanium containing compounds of the three dimensional ( $\text{Li}_{0.16}\text{La}_{0.62}\text{TiO}_3$  and  $\text{Li}_{0.10}\text{Ca}_{0.35}\text{La}_{0.40}\text{TiO}_3$ ) and two dimensional (2D) ( $\text{LiLaTiO}_4$  and  $\text{Li}_2\text{La}_2\text{Ti}_3\text{O}_{10}$ ) variants of the perovskite structure. The formation of compounds was characterized by powder X-ray diffraction. Compositional analyses were carried out using Field Emission Scanning Electron Microscopy and Energy Dispersive X-ray analysis. The 3-D perovskites,  $\text{Li}_{0.10}\text{Ca}_{0.35}\text{La}_{0.40}\text{TiO}_3$  and  $\text{Li}_{0.16}\text{La}_{0.62}\text{TiO}_3$ , were probed by static  $^6\text{Li}$ ,  $^7\text{Li}$  and  $^6\text{Li}$ ,  $^7\text{Li}$  MAS NMR.

$\text{Li}_{0.10}\text{Ca}_{0.35}\text{La}_{0.40}\text{TiO}_3$  was modelled in a hexagonal structure where A-site of the perovskite was occupied by Ca and La leaving 25% sites vacant while the Li was in a pseudo square planner environment leaving 83.3% sites vacant. However, the  $^7\text{Li}$  MAS NMR data indicated two different Li-sites. This apparent contradiction could be due to the fact that some of the Li moves out from the square planner site and goes into the A-site but in a distorted coordination environment as evidenced in the NMR. Further work is in progress to synthesize some more single phase Li-compounds of perovskite variants. The compounds will be structurally characterized and probed by dynamic NMR experiments involving relaxation studies to get more insight into the Li-ion conduction in these oxides.

## References

1. Dresselhaus, M. S.; Thomas, I. L. *Nature* **2001**, 414, 332.
2. Bruce, P. G.; Grenberger, S. A.; Hardwick, L. J.; Tarascon, J.-M. *Nature Materials* **2012**, 11, 19.
3. Chung, S.-Y.; Bloking, J. T.; Chiang, Y.-M. *Nature Materials* **2002**, 1, 123.
4. Ellis, B. L.; Makahnouk, W. R. M.; Makimura, Y.; Toghiani, K.; Nazar, L. F. *Nature Materials* **2007**, 6, 749.
5. Oumellal, Y.; Rougier, A.; Nazri, G. A.; Tarascon, J.-M. Aymard, L. *Nature Materials* **2008**, 7, 916.
6. Yang, S.; Sun, Y.; Chen, L.; Hernandez, Y.; Feng, X.; Müllen, K. *Scientific Reports* **2012**, 2, 1.
7. Goodenough, J. B. *J. Solid State Electrochem.* **2012**, 16, 2019.
8. Latie, L.; Villeneuve, G.; Conte, D.; Le Flem, G. *J. Solid State Chem.* **1984**, 51, 293.
9. Belous, A. G.; Novitsukaya, G. N.; Polyanetsukaya, S. V.; Gornikov, Yu. I. *Izv. Akad. Nauk SSSR, Neorg. Mater.* **1987**, 23, 470.
10. Inaguma, Y.; Chen, L.; Itoh, M.; Nakamura, T.; Uchida, T.; Ikuta, H.; Wakihara, M. *Solid State Commun.* **1993**, 86, 689.
11. Cussen, E. in *Functional Oxides*, eds. Bruce, D. W.; O'Hare, D.; Walton, R. I. Wiley, **2010**, p175-187.
12. Ibarra, J.; Várez, A.; León, C.; Santamaría, J.; Morres-Martínez, L. M.; Sanz, J. *Solid State Ionics* **2000**, 134, 219.
13. Fourquet, J, L.; Duroy, H.; Crosnier-Lopez, M. P. *J. Solid State Chem.* **1996**, 127, 283.
14. Inaguma, Y.; Itoh, M.; *Solid State Ionics* **1996**, 86-88, 257.
15. Bohnke, O.; Bohnke, C.; Sid'Ahmed, J. O.; Crosnier-Lopez, Duroy, H.; Le Berre, F. Fourquet, J. L. *Chem. Mater.* **2001**, 13, 1593.



16. Belous, A. G. *Ionics* **1998**, 4, 360.
17. Nakayama, M.; Ikuta, H.; Uchimoto, Y. Wakihara, M. *J. Mater. Chem.* **2002**, 12, 1500.
18. Inaguma, Y.; Chen, L.; Itoh, M.; Nakamura, T. *Solid State Ionics* **1994**, 70&71, 196.
19. Itoh, M.; Inaguma, Y.; Jung, W-H.; Chen, L.; Nakamura, T. *Solid State Ionics* **1994**, 70 & 71, 203.
20. Inaguma, Y.; Katsumata, T.; Yu, J.; Itoh, M. *Mater. Res. Soc. Symp. Proc.* **1996**, 453, 623.
21. Harada, Y.; Ishigaki, T.; Kawai, H.; Kuwano, J. *Solid State Ionics* **1998**, 108, 407.
22. Murphy, D. W.; Di Salvo, F. J.; Carides, J. N.; Waszczak, J. V. *Mat. Res. Bull.* **1978**, 13, 1395.
23. Tao, P.-C. *M. Sc. Thesis*, School of Science and Engineering, Reykjavik University.
24. Shukla, A. K.; Kumar, T. P. *Curr. Sci.* **2008**, 94, 314.
25. Whittingham, M. S. *MRS Bulletin* **2008**, 33, 411.
26. Padhi, A. K.; Nanjundaswamy, K. S.; Goodenough, J. B. *J. Electrochem. Soc.* **1997**, 144, 1188.
27. Fang, L.; Chowdari, B. V. R. *J. Power Sources*, **2001**, 97-98, 181.
28. Guo, H.; Zhao, H.; Jia, X. *Electrochem. Commun.* **2007**, 9, 2207.
29. Fan, X.-Y.; Ke, F.-S.; Wei, G.-Z.; Huang, L.; Sun, S.-G. *J. Alloys Compd.* **2009**, 476, 70.
30. Liu, S.; Li, Q.; Chen, Y.; Zhang, F. *J. Alloys Compd.* **2009**, 478, 694.
31. Daniel, C. *JOM J. Minerals, Metals & Materials Soc.* **2008**, 60, 43.
32. Choi, D.; Wang, W.; Yang, Z. in *Lithium-Ion Batteries, Advanced Materials and Technologies* eds. Yuan, J.; Liu, X.; Zhang, H. *CRC Press* **2011**, 17-18.
33. Dissanayake, M. A. K. L.; West, A. R. *J. Mater. Chem.* **1991**, 1, 1023.
34. Hong, H. Y. P. *Mater. Res. Bull.* **1978**, 13, 117.
35. Kuwano, J.; West, A. R. *Mater. Res. Bull.* **1980**, 15, 1661.

36. Aono, H.; Sugimoto, E.; Sadaoka, Y.; Imanaka, N.; Adachi, G. *J. Electrochem. Soc.* **1989**, *136*, 590.
37. Kanno, R.; Maruyama, M. *J. Electrochem. Soc.* **2001**, *148*, A742.
38. Mizuno, F.; Hayashi, A.; Tadanaga, K.; Tatsumisago, M. *Adv. Mater.* **2005**, *17*, 918.
39. Hayashi, A.; Minami, K.; Mizuno, F.; Tatsumisago, M. *J. Mater. Sci.* **2008**, *43*, 1885.
40. Kondo, S.; Takada, K.; Yamamura, Y. *Solid State Ionics* **1992**, *53*, 1183.
41. Takada, K.; Aotani, N.; Kondo, S. *J. Power Sources* **1993**, *43*, 135.
42. Kamaya, N.; Homma, K.; Yamakawa, Y.; Hirayama, M.; Kanno, R.; Yonemura, M.; Kamiyama, T.; Kato, Y.; Hama S.; Kawamoto, K.; Mitsui A. *Nature Materials* **2011**, *10*, 682.
43. Vallino, M.; Mazza, D.; *Proceedings of the First National Meeting on Engineering Materials, ASMI, Milano, Italy, 1983*, pp.387.
44. Kawai, H.; Kuwano, J. *J. Electrochem. Soc.* **1994**, *141*, L78.
45. Robertson, A. D.; Garcia Martic, S.; Coats, A. West, A. R. *J. Mater. Chem.* **1995**, *5*, 1405.
46. Grey, C. P.; Lee, Y. J. *Solid State Sciences* **2003**, *5*, 883.
47. Grey, C. P.; Dupré, N. *Chem. Rev.* **2004**, *104*, 4493.
48. Park, S.-H.; Kleinsorge, M.; Grey, C. P., Parise, J. B. *J. Solid State Chem.* **2002**, *167*, 310.
49. Meyer, B. M.; Leifer, N.; Sakamoto, S.; Greenbaum, S. G.; Grey, C. P. *Electrochem. Solid-State Lett.* **2005**, *8*, A145.
50. Heitjans, P.; Indris, S. *J. Phys. Condens. Matter.* **2003**, *15*, R1257.
51. Heitjans, P.; Schirmer, A. **1998**, *Diffusion in Condensed Matter*, ed. Kärger, J.; Heitjans, P.; Haberlandt, R. Berlin: Springer, p. 116-143.
52. Bloembergen, N.; Purcell, E. M.; Pound, R. V. *Phys. Rev.* **1948**, *73*, 679.
53. Wilkening, M.; Heitjans, P. *Chem. Phys. Chem.* **2012**, *13*, 53.

54. Heitjans, P.; Indirs, S.; Wilkening, M. *Diffus. Fundam.* **2005**, 2, 45.
55. Böhmer, R.; Jeffrey, K.; Vogel, M. *Prog. Nucl. Magn. Reson. Spectrosc.* **2007**, 50, 87.
56. Böhmer, R.; Jörg, T.; Qi, F.; Titze, A. *Chem. Phys. Lett.* **2000**, 316, 419.
57. Wilkening, M.; Mühle, C.; Jansen, M.; Heitjans, P. *J. Phys. Chem. B* **2007**, 111, 8691.
58. Wilkening, M.; Kuhn, A.; Heitjans, P. *Phys. Rev. B* **2008**, 78, 054 303.
59. van Wüllen, L.; Echelmeyer, T.; Meyer, H.-W.; Wilmer, D. *Phys. Chem. Chem. Phys.* **2007**, 9, 3298.
60. Emery, J.; Bohnke, O.; Fourquet, J. L.; Buzaré, J. Y.; Florian, P.; Massiot, D. *J. Phys.: Condens. Matter* **2002**, 14, 523.
61. París, M. A.; Sanz, J.; León, C.; Santamaría, J.; Ibarra, J.; Várez, A. *Chem. Mater.* **2000**, 12, 1694.
62. Hung, I.; Zhou, L.; Pourpoint, F.; Grey, C. P.; Gan, Z. *J. Am. Chem. Soc.* **2012**, 134, 1898.
63. Inaguma, Y.; Katsumata, T.; Itoh, M.; Morii, Y. *J. Solid State Chem.* **2002**, 166, 67.
64. Alonso, J. A.; Sanz, J.; Santamaria, J.; Leon, C.; Varez, A.; Fernandez-Diaz, M. T. *Angew. Chem. Int. Ed.* **2000**, 39, 619.
65. Stramiare, S.; Thangadurai, V.; Weppner, W.; *Chem. Mater.* **2003**, 15, 3974 & Yashima, M.; Itoh, M.; Inaguma, Y.; Morii, Y. *J. Am. Chem. Soc.* **2005**, 127, 3491.
66. Eckert, H. *Prog. Nucl. Magn. Reson. Spectrosc.* **1992**, 24, 159.
67. Freude, D.; Haase, J.; Diehl, P.; Fluck, E.; Günther, H.; Kosfeld, R.; Seelig (Eds.), J. *NMR – Basic Principles and Progress, Springer, Berlin.* **1993**, pp. 1–90.
68. Kirkpatrick, R. J.; Brow, R. K. *Solid State Nucl. Magn. Reson.* **1995**, 5, 9.
69. Jager, C.; Hartmann, P.; Witter, R.; M. Braun, M. *J. Non-Cryst. Solids.* **2000**, 263-264, 61.

70. Eckert, H.; Elbers, S.; Epping, J. D.; Janssen, M.; Kalwei, M.; Strojek, W.; Voigt, U.  
*Top. Curr. Chem.* 2004, 246, 195.
71. Duer, M. J. *Solid State NMR Spectroscopy*. 2002, Blackwell Science, Oxford.
72. Bjorkstam, J. L.; Villa, M. *Magn. Reson. Rev.* 1980, 6, 1.